IMPROVEMENT OF MECHANICAL PROPERTIES OF MESOPOROUS ULTRA LOW-*K* THIN FILMS AFTER NH_3 PLASMA TREATMENT

LI JINGHUI

(B. Eng., ECUST)

A THESIS SUBMITTED

FOR THE DEGREE OF MASTER OF SCIENCE

DEPARTMENT OF MATERIALS SCIENCE

NATIONAL UNIVERSITY OF SINGAPORE

2005

Acknowledgement

First of all, I would like to express my sincere gratitude to my supervisors, Dr. Chi Dong Zhi, Dr. Chiu Cheng Hsin and Dr. Zeng Kai Yang, for their continuous guidance and advice during the course of my research study. The scientific analysis methods and research skills imparted by them are beneficial to me for my future research work.

It is also my great pleasure to give my sincere thanks to the staff and students in Institute of Materials Research and Engineering (IMRE). I would like to give my special thanks to Mr. Wang Weide for training and help in plasma treatment, to Ms. Shen Lu for her kind help in nano-indentation test and scanning electron microscopy (SEM) measurement. I also want to thank Mr. Wang Lei, Mr. Liu Jun, Mr. Chum Chan Choy and Mrs. Doreen for their kind help.

In addition, I would acknowledge National University of Singapore (NUS) for providing me an opportunity to pursue my master degree and IMRE for providing equipments and scholarship, which have made this research possible.

Last but not least, I am indebted to my parents for their support, expectation and encouragement, which is a significant part behind the work.

Table of Contents

Summary

In this work, nano-indentation technique was applied to investigate the mechanical properties of porous low-*k* dielectric films with the particular emphasis on the beneficial effect of surface plasma treatment. While the nano-indentation characterization of the XLK^{TM} porous low-*k* thin films (with different porosities) clearly showed the correlation between the porosity and mechanical properties of porous low-*k* thin film that the mechanical properties deteriorate rapidly with increasing porosity, it was also found that surface plasma treatment of certain porous low-*k* films can improve the mechanical properties of the films significantly. NH_3 plasma treatment enhances the mechanical properties of porous low-*k* films by changing the near surface structure to form dense non-porous layers without affecting the porous structure in the bulk regions of the films. The dense layers were found to have much higher Young's modulus and hardness than those of the original porous low-*k* thin film. In order to confirm the formation of the dense layer at the surface, the structure of the plasma treated porous low-*k* thin films was investigated using transmission electron microscopy (TEM). A very thin dense layer was indeed observed under TEM.

To understand the mechanism of the formation of porous low-*k* thin films, time of flight--secondary ions sass spectrometry (TOF-SIMS) was conducted on the plasma treated porous low-*k* films to analyze the change of element concentration with the depth of porous low-*k* thin films. It was found that carbon depletion occurred at the near surface area with longer treatment time leading to deeper carbon depletion. At the same

time, it was also found that nitrogen peak appeared in the near surface region. The nitrogen peak moves deeper into the bulk region with increasing plasma treatment time. Based on these experimental observations, we propose following formation mechanism for the NH_3 plasma induced dense surface layer: (1) after plasma generation, energetic radicals and ions quickly diffuse into open nano-pores in the surface region and interact with the walls, causing the collapsing of the open nano-pores; (2) radicals and ions continuously diffuse into the skin layer and react with the low-*k* thin film to form carbon-depleted and nitrogen-incorporation layer; (3) the bombardment of ions and chemical reaction of H^+ and N^+ with porous low-*k* thin films induced the formation of dense layer. It is important to point out that the presence of the dense surface layers appears to protect the bulk regions of the films from plasma damages since it was found that the chemical structure in the bulk regions of the plasma treated porous low-*k* thin films remained unchanged as revealed by Fourier transformation infrared (FTIR) spectrometry characterization.

Conclusively, with the formation of the NH_3 plasma induced non-porous dense surface layer, the increased young's modulus and harness, coupled with the minimum damage to the bulk properties of the plasma treated low-*k* films, would make chemical mechanical polishing (CMP) process more feasible.

List of Tables

List of Figures

Nomenclature

Notation

k	Dielectric constant
R	Wire resistance
C	Parasitic capacitance
ρ	Resistivity of interconnect material,
ε	Permittivity of inter-layer dielectric (ILD) material
P	Loading
h	Indentation depth

Abbreviation

CMP	Chemical Mechanical Polishing
TEM	Transmission Electron Microscopy
FTIR	Fourier Transformation Infrared spectrometry
ILD	Inter-Layer Dielectric
ITRS	International Technology Roadmap for Semiconductors
MSQ	Methyl-Silses-Quioxane
PECVD	Plasma Enhanced Chemical Vapor Deposition
IUPAC	International Union for Pure and Applied Chemistry
HSQ	Hydrogen-Silses-Quioxane
SOD	Spin on Deposition
ALCVD	Atomic Layer Chemical Vapor Deposition
HOSP	Hybrid-Organic-Siloxane-Polymer
DMA	Dynamic Mechanical Analysis

TMA	Thermo-Mechanical Analysis
RF	Radio Frequency
DC	Direct Current
CVD	Chemical Vapor Deposition
CSM	Continuous Stiffness Measurement
AFM	Atomic Force Microscope
FSG	Fluorine-doped Silicate Glass
IC	Integrated Circuits
RIE	Reactive Ion Etching
PALS	Positronium Annihilation Lifetime Spectroscopy
TOF-SIMS	Time-of-flight Secondary Ion Mass Spectrometry

Chapter 1. Introduction

1.1 Background

In order to improve the performance of integrated circuits, the feature size in Si-based integrated circuits has been reduced to 100 nm range in recent years. Further improvement to reach the 65 nm technology node is currently under development in the leading semiconductor manufacturing companies such as Taiwan Semiconductor Manufacturing Cooperation (TSMC), International Business Machines Cooperation (IBM) and Chartered Semiconductor Manufacturing Cooperation (CSM). There are many benefits of smaller feature size. A major benefit of smaller feature size is a higher clock frequency [1]. This is demonstrated in Fig. 1.1, which depicts the variations of the clock frequency with the feature size of the integrated circuit for four different material combinations of interconnects/insulators, namely Cu/low-*k*, Al/low-*k*, Cu/SiO_2, and Al/SiO_2. In all of the cases, the clock frequency increases by at least two times when the feature size is reduced from 250 to 50 nm: the clock frequency can increase from 800 MHz to as high as 3100 MHz for the case of the Cu/low-*k* stack.

While the continuous miniaturization has been the main approach employed to enhance the performance of the integrated circuits, there are several new issues arising from the aggressive scaling of the device feature size. One of the issues is the *RC* interconnect time delay resulting from the wire resistance *R* of the interconnects and the parasitic capacitance *C* of the insulators [2, 3].

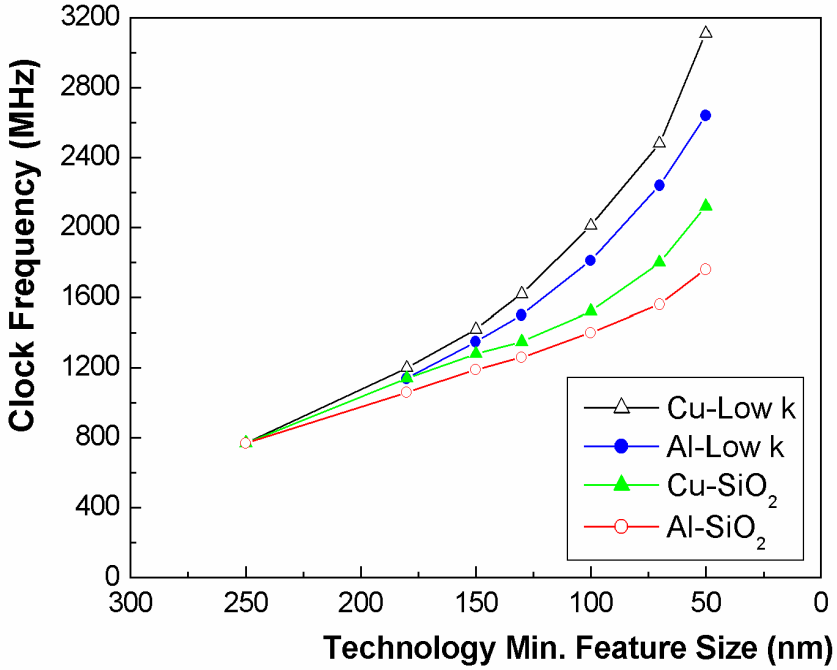

Fig. 1.1 Clock frequency versus integrated-circuits (IC) feature size.

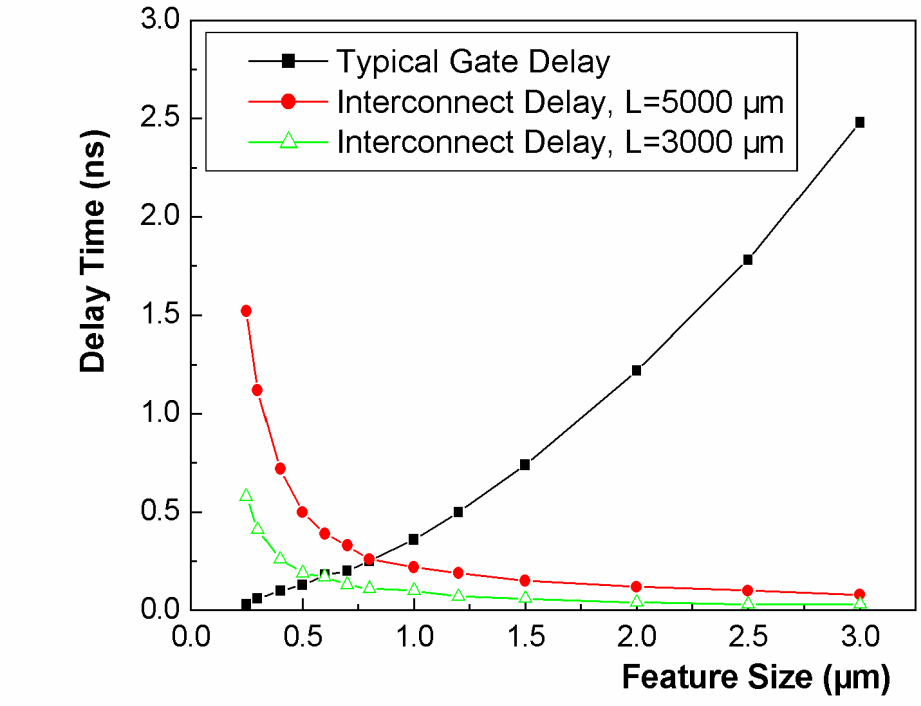

Fig. 1.2 Resistance-capacitance (*RC*) delay time versus integrated circuits (IC) feature size.

Fig. 1.2 shows the two types of delay which affect the overall time delay in integrated circuits [1]. One is *RC* delay. The other is the gate delay. As shown in Fig. 1.2, the *RC* delay has become one of the main factors limiting the improvement in device operation speed, overwhelming the reduction in the gate delay, for the sub-micron technology nodes. Therefore, the total time delay decreases first with decreasing feature size (for > 1 micron), and then increases due to the rapidly increasing interconnect delay as the feature size is further reduced down into sub-micron regime [2-4].

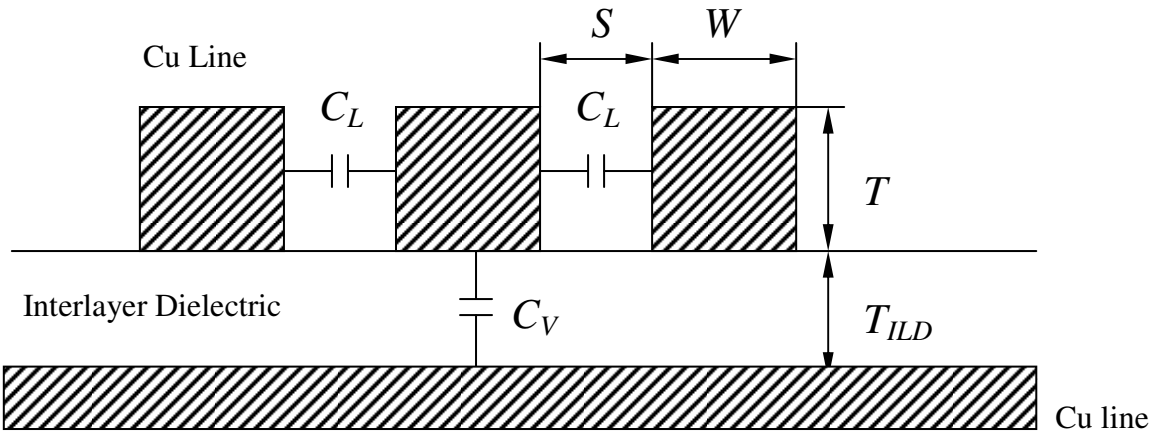

Fig. 1.3 Basic structure of interconnects and inter-layer dielectrics [5].

For a given feature size, the *RC* time constant (wire resistance *R* and parasitic capacitance *C*) is determined by interconnect and dielectric materials. A typical cross-section of interconnects and dielectric insulators is shown in Fig. 1.3. The shadow area represents the Cu line and the white area represents the dielectrics between Cu lines. The *RC* time constant is simply the product of the total resistance R_I of interconnects per unit length and the total capacitance C_T of the insulators per unit length [5]. It is expressed in the following equations:

$$RC = R_I C_T \tag{1-1}$$

The interconnect resistance R_I is given by

$$R_I = \frac{R}{L} = \frac{\rho}{WT} \tag{1-2}$$

with ρ as the resistivity of interconnect material, W as the width of interconnects, and T as the thickness of interconnect. The total capacitance (per unit length) is the sum of the capacitance between the Cu lines C_L and the intra-layer capacitance C_V and is given by

$$C_T = C_V + 2\ C_L \tag{1-3}$$

The intra-layer capacitance C_V and the inter-line capacitance C_L are expressed to be

$$C_V = \frac{C}{L} = \varepsilon \frac{W}{T_{ILD}} \tag{1-4}$$

$$C_L = \varepsilon \frac{T}{S} \tag{1-5}$$

where T_{ILD} is the thickness of interlayer dielectric thin film, S is the distance between the lines, and ε is the permittivity of inter-layer dielectric (ILD) material. Substituting the Eqs. (1-2), (1-3), and (1-4) into Eq. (1-1) yields

$$RC = R_I C_T = \rho\varepsilon\left(\frac{1}{TT_{ILD}} + \frac{1}{WS}\right) \tag{1-6}$$

In most of the cases, the thickness T of the interconnect wires and the thickness T_{ILD} of the interlayer dielectric thin film remain almost unchanged, while the feature sizes W and S decrease significantly as the technology advances. As a consequence, the RC time delay increases significantly if the same interconnect materials and dielectric materials are used. In order to reduce the large RC time delay, which increases rapidly with the decreasing feature size, Cu has been introduced as the interconnect material to replace Al, and low-k dielectrics has been developed to replace SiO_2. The reduction in

resistivity ρ by the use of Cu and the reduction for the dielectric constant ε by the use of low-*k* dielectrics help to lower the *RC* delay, thus allowing for high-speed device operation [5-7].

Besides the increase in the *RC* time delay, there are two other problems arising from the reduction of feature sizes: increased crosstalk and high power consumption [8]. The increased crosstalk is due to the fact that it is proportional to intra-layer capacitance C_L through

$$\frac{\Delta V}{V} \propto C_L \propto \varepsilon \tag{1-7}$$

where ΔV is the voltage drop and V is the power supply voltage.

As suggested in Eq. (1-5), C_L increases as the feature size decreases. In other words, decreasing the feature size leads to higher crosstalk. In order to decrease the signal crosstalk between two neighboring wires, it is necessary to reduce the C_L. In order to reduce C_L, it is inevitable to use dielectrics with lower dielectric constant.

The problem of high power consumption can be understood as follows. There are two elements contributing to the power consumption. One is the dynamic power given by

$$P = \alpha C V^2 f \tag{1-8}$$

where P is the dynamic power consumption, α is the wire activity, V is the power supply voltage, f is the frequency, C is the sum of the output and input capacitance of the transistors and the capacitance introduced by the wire itself. The dominance of wire capacitance and the dynamic power dissipation is influenced significantly by the dielectric constant of the ILD materials between the wires. Therefore, low dielectric

constant is required for lower dynamic power consumption. The other contributor to the power consumption is the static power, which is related to the leakage current between wires. In order to reduce the static power consumption, low leakage is an additional and important requirement for the ILD dielectric materials [8].

It is obvious that, in addition to the use of Cu as interconnecting wire material, low-*k* ILD dielectric materials must be developed to replace conventional SiO_2 (*k*~3.9) in order to solve the above three problems. Table 1.1 summarizes the expected progress for the interconnect technology, including the requirement for the *k* values of the ILD dielectrics, listed in the international technology roadmap for semiconductors (ITRS) of 2001 [9]. It must be noted that, because of the presence of other dielectric layers that are necessary to improve process control or to protect the low-*k* material in the dielectric stack during processing, it is necessary to consider an effective *k* value, which is a combination of the *k* value of the low-*k* dielectrics and those of all other dielectrics between the wires [8]. Therefore, the desired effective *k*-value for each technology node is also specified in ITRS. The effective *k* value will be higher than the actual *k* value of the ILD material due to process interactions and the presence of other thin dielectric layers.

According to the ITRS, further reduction of the *k* value of ILD materials is still needed for the future technology node from the current level. Currently, the *k* value of the most advanced ILD technology is 2.7~3.0. Since *k* is determined by polarizability, which is related to the density of molecular bonds, polymeric materials with their low mass density tend to have the lowest *k* values, in the range of 2.5~3.5. Below this range,

it is difficult to further reduce the dielectric constant by using fully dense materials. The solution to the limit is the porous ultra low-*k* (*k* less than 2.2) ILD materials [10, 11].

The requirements for the dielectric constant in future technology nodes, coupled with practical limit on fully dense materials in reducing *k* values, has triggered tremendous development efforts to develop porous low-*k* ILD materials. Remarkable progress has been made in reducing the *k* values [12]. However, the introduction of the porous low-*k* ILD in the integrated circuits faces a range of process integration challenges, including the difficulty to form an effective thin Cu diffusion barrier on porous surface [13], the interaction of the porous low-*k* materials with chemicals/free radicals/moistures during various processes (e.g. plasma etching, chemical cleaning, chemical mechanical polishing (CMP)), and the intrinsically weak mechanical strength of the porous low-*k* materials [14, 15]. The weak mechanical strength is particularly problematic since it makes the subsequent CMP and packaging process extremely difficulty. To overcome these difficulties, it is pivotal to develop innovative methods that can improve the mechanical properties of porous low-*k* thin films without causing significant increase in the *k* value to meet the requirements for being compatible with the CMP and packaging processes [16].

Table 1.1 Characteristic numbers for future technology nodes relating to dimensions and material characteristics from the ITRS 2001 roadmap [9].

Year of Production	**2001**	**2004**	**2007**	**2010**	**2013**	**2016**
DRAM 1/2 pitch (nm)	130	90	65	45	32	22
MPU/ASIC 1/2 Pitch (nm)	150	90	65	50	35	25
MPU printed gate length (nm)	90	53	35	25	18	13
MPU physical gate length (nm)	65	37	25	18	13	9
Local wiring						
Local wiring pitch (nm)	350	210	150	105	75	50
Total interconnect capacitance (fF/mm)	192	169	148	127	118	114
Interconnect RC delay 1mm line (ps)	86	198	342	565	970	2008
Intermediate wiring						
Intermediate wiring pitch (nm)	450	265	195	135	95	65
Total interconnect capacitance (fF/mm)	197	173	154	130	120	116
Interconnect *RC* delay 1mm line (ps)	53	127	198	348	614	1203
Global Wiring						
Global wiring pitch (nm)	670	460	290	205	140	100
Total interconnect capacitance (fF/mm)	211	186	167	143	133	128
Interconnect *RC* delay 1 mm line (ps)	21	37	79	131	248	452
Bulk *k* value	2.7	2.4	2.1	1.9	1.7	1.6
Effective *k* value	3-3.6	2.6-3.1	2.3-2.7	<2.1	<1.9	<1.6

1.2 Porous Low-*k* Thin Films

In the last decade, there have been tremendous efforts in developing low-*k* thin films and integrating them with Cu interconnects into advanced integrated circuits. Several generations of low-*k* thin films, including ultra low-*k* thin films with the *k* values below 2.0, have been successfully developed over last several years. While a low dielectric constant is the utmost criteria for the application of low-*k* thin films, the low-*k* thin films also need to meet other strict requirements for process-integration, which include sufficiently high thermal and mechanical stability, good adhesion to other interconnect materials, low moisture absorption, and low cost for processing [17].

Generally, materials with a high density of strong chemical bonds tend to be structurally stable. However, the strong chemical bonds are often highly polarizable, which leads to a high polarizability and consequently a high dielectric constant of the material [18]. For instance, due to the high density of the chemical bonds in SiO_2, the stiffness and the thermal stability of the material are high. The high density of bonds, however, causes a large atomic polarizability and therefore a rather high dielectric constant of 4.2. The dielectric constants of organic polymeric materials, on the other hand, are low because of lower dielectric constant due to lower material (i.e. chemical bond) density and lower bond polarizability. However, most organic polymers cannot withstand high thermal exposure, and few organic low-*k* polymers show reasonable stability above 400 蚓[19].

As stated in the previous section, *k* is determined by polarizability, which is related

to the density of molecular bonds, polymeric materials with low mass density tend to have the lowest k values, in the range of 2.5~3.5. Below this range, it is difficult to further reduce the dielectric constant of fully dense materials. To achieve even lower k values, introducing porosity into the insulator has become the dominant strategy recently. The main approach is to decrease the material density by incorporating meso- and/or micropores into a material network. According to the International Union for Pure and Applied Chemistry (IUPAC) definition, mesoporous typically describes materials containing pores of 2~50 nm in diameter, whereas microporous is used to describe materials with pores less than 2 nm in diameter [20].

The porosity P is defined as the fraction of total volume of the pores in the film

$$P = \frac{V_p}{V} \tag{1-9}$$

where V_p is pore volume and V is total volume of the material. The porosity P of a material can significantly affect the dielectric constant k of the material with the effect typically being approximated by the following simple formula

$$\ln k_c = (1-P)\ln k_1 + P \ln k_2 \tag{1-10}$$

where k_1 and k_2 are the permittivities of the "dense" material and that of air, respectively, and k_c is the resulting dielectric constant [21].

1.2.1 Classification of Porous Low-*k* Materials

There are many kinds of porous low-k materials. According to their host matrix materials, the low-k materials can be classified into four categories: porous organic materials, porous inorganic materials, porous organic-inorganic materials, and

amorphous carbon [22]. These materials are briefly discussed in the following sections.

1.2.1.1 Porous Organic Low-*k* Materials

Organic polymers can be categorized into two different groups based on the polarity of the molecules in the polymers. The first group is non-polar polymers that contain molecules with almost purely covalent bonds. The dielectric constant of this type of polymers can be estimated by the Clausius–Mossotti (Lorentz–Lorenz) equation

$$3\varepsilon_0 \frac{\varepsilon_r - 1}{\varepsilon_r + 2} = N\alpha \tag{1-11}$$

where N is the number density of molecules, ε_r is the relative permittivity, ε_o is the permittivity of vacuum, and α is the polarization constant.

The second group is the polar polymers that contain atoms of different electronegativity and accordingly polarized chemical bonds. The high polarization in the bonds affects the dielectric constant in two aspects. First, the polarization causes higher dielectric constants. Second, since the polarization is affected by the temperature and the frequency, the dielectric constant depends on the temperature and the frequency at which the constant is measured [23].

Among the organic polymers, the dielectric constants of those containing the aliphatic C-C, C-H, and C-N bonds are generally the lowest. Therefore, they may provide the lowest k value. However, the aliphatic bonds are unstable at temperature is larger than 300 蚓and in some cases at even lower temperatures. Therefore, only organic polymers composed of non-aliphatic C–C, C–O, C–N, and C–S bonds, aromatic structures, and cross-linked or ladder structures can withstand the temperatures

necessary for interconnect technology (450~500 ℃). The thermal stability as well as the dielectric constant can be further improved by fluorination of the polymers because the C–F bond is stronger than C–H and fluorination reduces the polarization of the chemical bonds [23]. The dielectric constants of most of the organic low-*k* films with sufficient thermal stability are in the range between 2.6 and 2.8 [22].

The dielectric constant of the organic polymer can be lowered by producing pores in the polymers. The application of some of these porous polymeric films to the interconnect technology, however, is limited because of their low thermal stability, low stiffness, and incompatibility with the traditional processes developed for SiO_2 based dielectrics [19, 23].

1.2.1.2 Porous Inorganic Low-*k* Materials

The inorganic low-*k* materials are mainly silica-based. The silica-based porous low-*k* materials have the tetrahedral basic structure of SiO_2. Silica has a molecular structure in which each Si atom is bonded to four oxygen atoms, and each oxygen atom to two silicon atoms ($SiO_{4/2}$). The structure is shown in Fig. 1.4(a). Each silicon atom is at the center of a regular tetrahedron of oxygen atoms. All types of silica are characterized by a high density and high chemical and thermal stability. The density of different silica types varies between 2 and 3 g/cm^3. In particular, the density of amorphous silica films, used in microelectronics, is about 2.1~2.3 g/cm^3. The dielectric constant of silica is about 4 when measured at low frequency. The dielectric constant falls to about 2.15 when the frequency is raised to the range of visible light. The

variation of the dielectric constant with the frequency is mainly caused by the high polarizability of the Si-O bonds. The dielectric constant can be lowered by using the F-doped silica glasses (FSG) in which the Si–O bonds are replaced by the less polarizable Si–F bonds. Another approach is to dope the silicate glasses with CH_3 groups to lower the *k* value. Moreover, both fluorine and carbon increase the inter-atomic distances or ‘‘free volume’’ of silica, which provides an additional decrease of dielectric constant [23].

The elementary unit of C-doped silica glasses is presented schematically in Fig. 1.4. Fig. 1.4(a) shows the basic unit of silica. The C-doped silica is shown is Fig. 1.4(b). The uncross-linked C-doped silica is shown in Fig. 1.4(c). Fig. 1.4(d) shows these elementary units form long chains with different degrees of cross-linking. Typical densities of C-doped silica glasses are between 1.2 and 1.4 g/cm^3, which is significantly lower than SiO_2. C-doped silica films have dielectric constants close to 2.6–3. The *k* value of the material depends on the number of CH_3 groups built into the structure since they lower both polarity and density of the material by steric hindrance [22].

Porous silica low-*k* thin film offers two major advantages: high thermal stability and low thermal expansion coefficient. Its thermal conductivity is higher than that of the organic porous low-*k* thin film. However, the silica-based low-*k* material requires high porosity to achieve a low dielectric constant since the value of *k* of silica is as high as 4.2. The high porosity causes poor mechanical properties and cracking. The high porosity also means that a diffusion barrier layer is needed in order to prevent the Cu in the interconnecting wires from diffusing into the surrounding dielectric film. However, the

diffusion barrier layer makes the integration process more complicated and affects the effective dielectric constant of the whole stack [24-26].

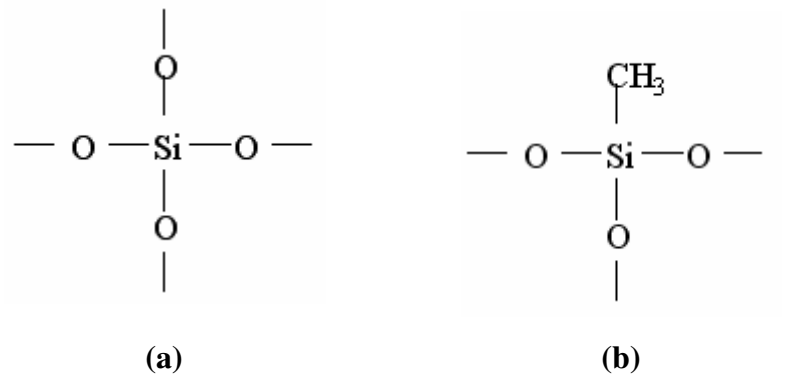

(a) **(b)**

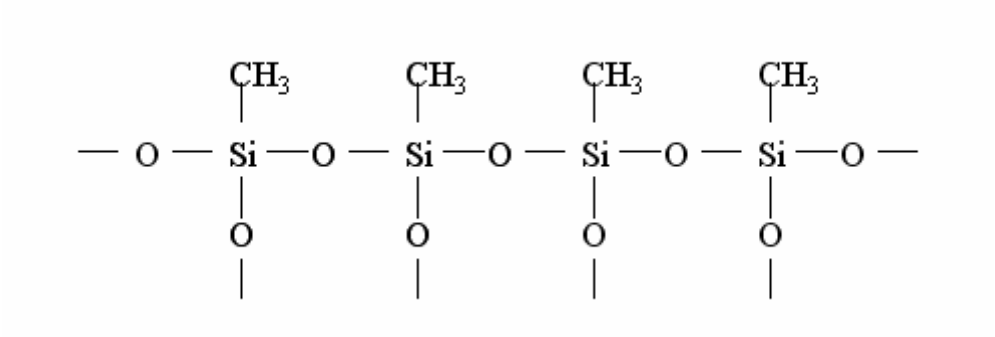

(c)

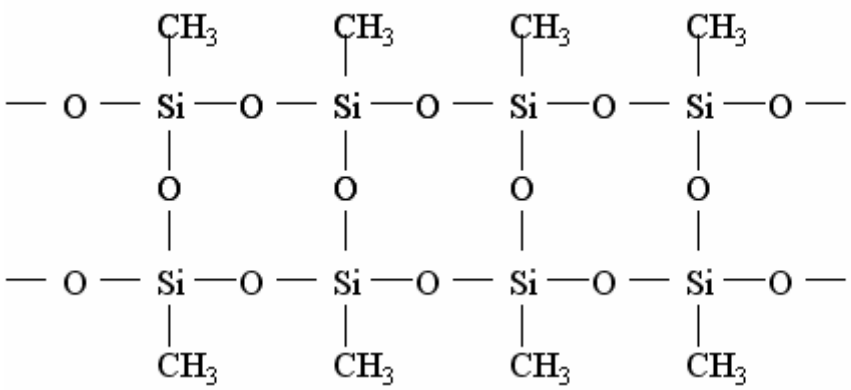

(d)

Fig. 1.4 Elementary unit of **(a)** SiO_2 **(b)** doped silica glass and schematic bonding structure **(c)** without and **(d)** with cross-linking.

1.2.1.3 Porous Organic-inorganic Low-*k* Materials

Organic-inorganic low-*k* materials refer to silsesquioxanes with the empirical formula $(R\text{-}SiO_{3/2})_n$ where R refers to a substitute. The most common representative structures of silsesquioxanes are a ladder-type structure and a cage structure containing eight silicon atoms placed at the vertices of a cube (as shown in Fig. 1.5). The substitutes (R) can be hydrogen, alkyl, alkenyl, alkoxy, and aryl. The organic group R helps many silsesquioxanes dissolve in common organic solvents. The organic substitutes also lead to low density and thus low dielectric constant.

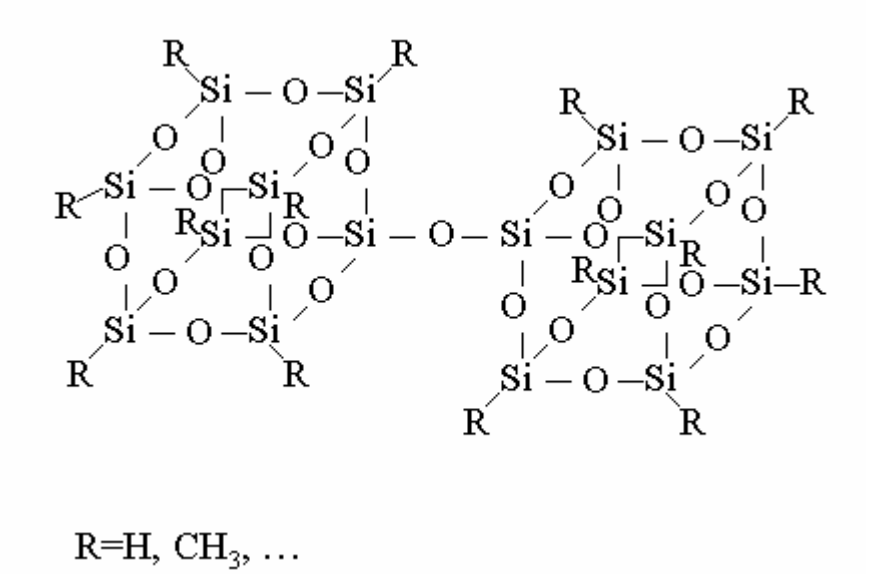

Fig. 1.5 Structure of elementary units of silsesquioxane dielectric materials [22].

The silsesquioxane-based materials for microelectronic applications are mainly hydrogen-silsesquioxane (HSQ) and methyl-silsesquioxane (MSQ). The basic units of these two materials are the cage structure as depicted in Fig. 1.5. The dielectric constant for MSQ and HSQ material is 2.8 and 3.0, respectively. The dielectric constants of MSQ materials are lower than that of HSQ because of the following two reasons. First, the

group in MSQ is CH_3 and it is bigger than the group (H) in HSQ. Thus the density of MSQ is lower than that of HSQ. Second, the polarizability of the Si-CH_3 bond in MSQ is lower as compared to that of Si-H bond in HSQ.

Porous MSQ low-k thin films have attracted attention of many researchers because their mechanical and thermal stability are better than that of purely organic or inorganic materials. However, with the presence of nano-pores, porous MSQ also faces integration and reliability challenges such as CMP compatibility [23, 27, 28].

1.2.1.4 Amorphous Carbon

The last kind of low-*k* materials is the so-called "amorphous carbon" [29, 30]. The material is usually obtained by plasma-enhanced chemical vapor deposition methods using a discharge with fluoro-carbon gases [31, 32]. This material is not attractive because of its poor thermal stability and mechanical properties.

1.2.2 Fabrication of Porous Low-*k* Films

There are two major methods for fabricating porous low-*k* thin films, namely spin on deposition (SOD) and chemical vapor deposition (CVD). The two methods are briefly discussed in this section.

1.2.2.1 Spin on Deposition (SOD)

The spin-on deposition technique can deposit thin films with good planarization and gap filling. The film materials can be inorganic and organic films, while the dielectric precursors should be in soluble form. Thin film deposition is performed by

dispensing a liquid precursor at the center of the substrate, which is placed on a spinner. This is commonly done at room temperature and ambient pressure. Rotation of the substrate creates centrifugal forces that ensure a uniform distribution of material on the substrate. The thickness of the coating is a result of the balance between the centrifugal forces (dependent on the rotation speed) and the viscous forces that are determined by the viscosity of the solution. After spinning, the coating undergoes a sharp increase in viscosity and transforms into a "wet gel". The wet gel is a hard substance yet consisting of a liquid and a solid component. The subsequent step is baking at temperature below 250 蚓to remove solvents, which cause the weight and the volume of the film to reduce by as much as 50%. The baking of the wet gel is a critical process for promoting porosity in the film. Finally, sintering temperature varying from 350 to 600 蚓is required to obtain a stable film. The cure process induces the final cross-linking of the polymer chains and results in a mechanically stable film structure [33, 34].

With SOD, the introduction of pores into the film is typically done by using sacrificial "nano-particles" that are desorbed during the film cure process. The nano-particles are added in the dielectric precursor. The stability of these particles is adjusted so that the particles are not affected by the coating drying step, and they can be removed by pyrolysis during the final film sintering or cure process. In ideal cases, the size and the amount of nano-particles in the precursor solution determine the pore size and the final porous fraction in the film. In other words, the pore size and the porosity can be controlled independently [35, 36].

1.2.2.2 Chemical Vapor Deposition (CVD)

The fundamental principles of CVD involve a wide variety of scientific and technical principles including gas phase reaction chemistry, thermodynamics, heat and material transfer, fluid mechanics, surface and plasma reactions, thin film growth mechanism, and reactors engineering [37]. It is now well understood that the gas phase reactions produce active intermediate and structural units, which are then transported to the growing layer above the film surface by convection. The lifetime and concentration of the active intermediates in the gas phase is proportional to the reactor volume (V) and inversely proportional to the internal surface area (S) of the reactor including the wafer surface because the chain-branch reactions are mainly terminated by the surface [38-40]. If the S/V ratio is too high, the intermediates, which are crucial for film formation, are deactivated on the reactor and sample surface. As a result, no thin film growth is observed. If the S/V ratio is too small, the concentration of intermediates in the gas phase is too high, which may result in polymerization reactions to form powder-like product. Only in the optimal S/V range, the concentration of intermediates in the gas phase is suitable for the growth of a solid film [41]. Therefore, any changes decreasing the concentration of intermediate in the gas phase, which results in limited incorporation of agglomerates in the gas phase, shifts the process from the region of solid film formation to that of porous film formation. [42].

1.3 Integration of Cu/Porous Low-*k*

Copper and low-*k* materials have replaced traditional aluminum and SiO_2 as the

interconnect and interlayer dielectric materials, respectively, since the new combination can lead to higher device performance by reducing the *RC* time delay. The challenge of using Cu in the integrated circuits is that it is hard to etch Cu and the byproduct of Cu etching process is solid while the byproduct of Al etching process is volatile. The solid byproduct will cover the surface of Cu and prevent the Cu from being etched. To overcome these problems, engineers invented the method of damascene.

1.3.1 Damascene Process

Before we introduce the damascene process, we first briefly mention the conventional scheme for fabricating Al interconnects and SiO_2 dielectric material and explain the difficulty of using the conventional technique when the interconnect material is Cu. The conventional processing scheme for Al interconnects is shown in Fig. 1.6. First, the Al is deposited on the wafer and photoresist is deposited on the Al surface. Then, the photoresist is exposed and developed to form positive pattern on the Al. After the development of photoresist, the Al where it is not protected by the photoresist is removed by etch process. The following last two steps are dielectric deposition and planarization. However, this conventional process is not suitable for Cu because it is hard to etch Cu and the byproduct of Cu etching process is solid as mentioned in the last paragraph.

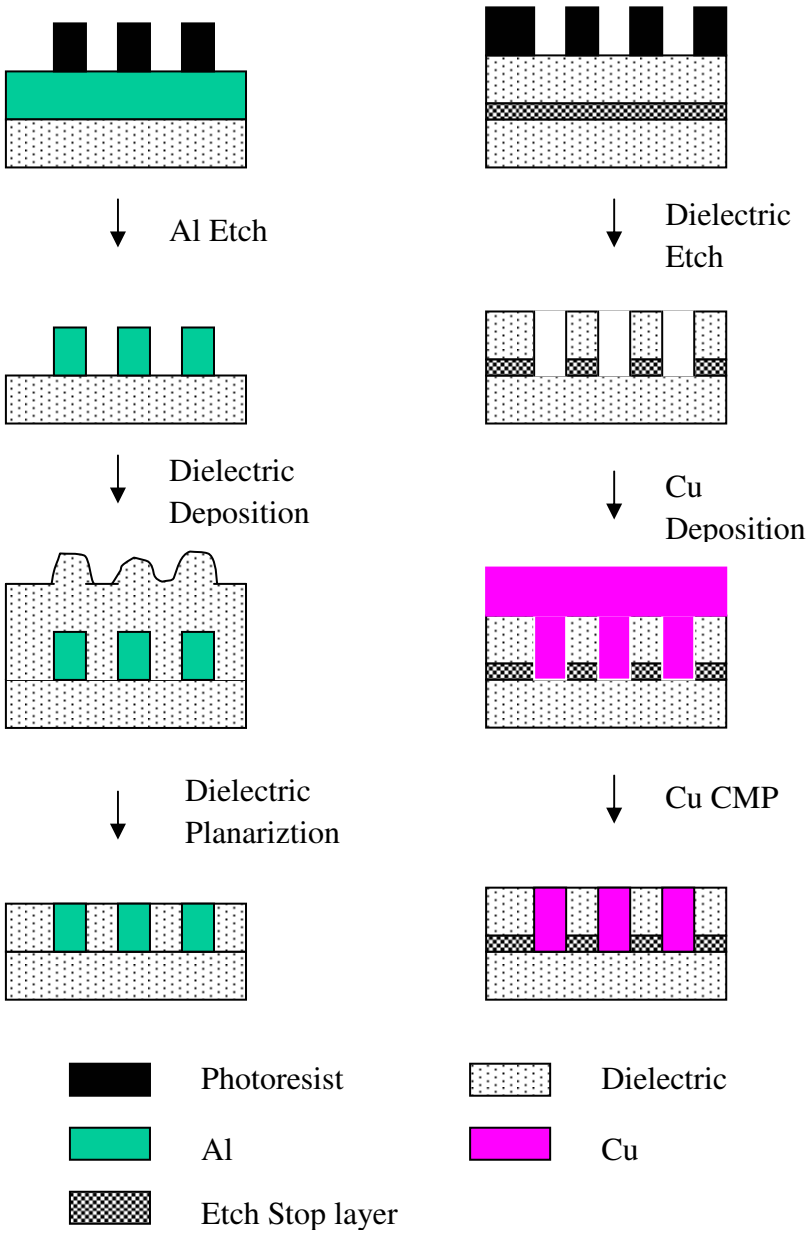

Fig. 1.6 Interconnect fabrication process. Left: conventional standard process. Right: single damascene process.

The damascene process is introduced to resolve the difficulty in processing copper interconnects [33]. A typical damascene process is illustrated in Fig. 1.6. First, inter-metal dielectric layer is deposited and photoresist was patterned on the surface of dielectric layer. Then the areas where the dielectric material is not protected by

photoresist are removed in the subsequent dielectric etching process. The process is followed by the Cu deposition to fill the open areas generated by the etching process until Cu covers the whole wafer surface. Subsequent CMP process removes the excess Cu. The damascene structure introduces a whole new set of materials and processes different from the standard aluminum and SiO_2 interconnect technology [33].

1.3.2 Barrier Layers

For traditional aluminum-based metallization, titanium (Ti) and its nitride (TiN) have been most commonly used as a diffusion barrier/adhesion promoter to improve the wettability and mechanical stability of the aluminum interconnects [43]. In the case of copper, the need for a diffusion barrier is even more critical in view of the high diffusivity of copper in silicon and silicon dioxide. The presence of copper in silicon dioxide results in highly adverse effects and causes serious device degradation and failure. Therefore, an effective diffusion barrier material is needed in order to prevent the Cu from diffusing and intermixing with adjacent dielectrics. The diffusion barrier layers must be thin and they have to be able to be deposited conformally on surfaces of the patterned dielectrics after the dielectric etching process. Such diffusion barrier layers are further required due to the poor adhesion between copper and various low-*k* materials.

Since the diffusion process is controlled by the melting temperature of the material, it is desirable to select barriers with a high melting temperature. To perform effectively, the barrier layers must be continuous, without pinholes or defects to minimize the

formation of diffusion path. Furthermore, as the feature size continues shrinking, the barrier materials must provide the required performance of preventing Cu diffusion at reduced thickness in order to keep the space availability for the actual copper conductor. The need to reduce the thickness of the barrier layer means stringent requirements on integrity, continuity, conformality and stability of the barrier.

There are three dominant diffusion barrier failure mechanisms. First, the barrier can fail because of a metallurgical or chemical reaction with the copper and/or the substrate. The second failure mechanism is a barrier can lose containment integrity if diffusion of copper along grain boundaries. The third mechanism is diffusion of copper or substrate atoms through bulk defects in the barrier itself.

An effective barrier layer must not react with copper or the substrate under the thermal, mechanical and electrical conditions encountered in subsequent processing steps or the normal operating conditions. A good candidate satisfying these criteria is tantalum (Ta) and its nitride or silicide. The problem of Ta diffusion barrier is that Cu can diffuse through grain boundaries and defects in the Ta layer [44]. The problem can be resolved by employing TaN. The TaN material contains smaller N atoms in the interstitial sites of the close-packed Ta crystal structure. The N atoms help blocking Cu diffusion; accordingly, increasing the nitrogen content reduces the diffusivity of Cu in the barrier [45]. In addition to the advantage of slower Cu diffusion, adhesion between TaN with dielectric films is also stronger than that of Ta with dielectric films [46, 47].

1.3.3 Integration Issues with Porous Low-*k* Thin Films

With the introduction of pores, the mechanical properties of the porous low-*k* thin film are degraded. However, the CMP process requires that low-*k* material to be sufficiently strong to withstand the shear stress to avoid delamination or crack in the fragile porous low-*k* thin films. In addition to the mechanical failure during the CMP process, there are also other challenges. For example, the open pores at the surface may cause some troubles in depositing continuous and smooth barrier layer. The pores provide paths for Cu diffusion; thus, porous low-*k* thin films are more vulnerable to Cu diffusion [48, 49]. The voids in the thin film may adsorb water, resulting in an increase of the effective dielectric constant. Water absorbed by the porous low-*k* thin films can be physisorbed, weakly bonded, or tightly bonded. Physisorbed water can be easily desorbed at temperature below 200 蚓| Weakly bonded water can be desorbed around 400 蚓| Tightly bonded moisture is irreversible and has a detrimental effect on the dielectric properties of the films [50-52]. The low-*k* materials are also vulnerable during the ashing and stripping process. This may cause an increase of moisture absorption and dielectric constant [53, 54]. Therefore, it is necessary to seal the open pores on the surface and improve the mechanical properties of porous low-*k* thin films to avoid above problems.

1.4 Plasma Treatment Effects

How to integrate the porous low-*k* materials into the device becomes one of the major bottlenecks in developing future technology nodes in semiconductor industry.

Researchers have used different types of plasma treatment to improve the properties of low-*k* materials, including O_2, N_2+O_2, H_2, N_2+H_2, and NH_3. These plasma treatments are discussed in the following sections.

1.4.1 O_2 Plasma Treatment

Researchers modified Si-O-C and α-SiC:H dielectric films by O_2 plasma treatment to enhance the atomic layer chemical vapor deposition (ALCVD) growth of TiN barrier layer on it [55]. The O_2 plasma increases the OH group density on the surface of the low-*k* material, which improves the quality of the TiN films. The oxygen diffuses mainly through the micropores of the low-*k* dielectric. Ion bombardment provides additional densification of the film surface so that the oxygen diffusion through the micropores can be limited. Therefore, the O_2 plasma treatment will change the characteristics of the surface of the thin film. The ALCVD TiN on the porous low-*k* thin film with O_2 plasma treatment is smoother and more continuous than that on an untreated low-*k* thin film. However, O_2 plasma treatment has drawbacks such as shrinkage and deep oxidation of porous low-*k* thin films. The oxygen plasma may remove Si-CH_3 and Si-H resulting in an increased water adsorption and a higher dielectric constant. The drawbacks of O_2 plasma treatment can be partially resolved by adding bias to the substrate [56].

1.4.2 H_2 Plasma Treatment

The H_2 plasma treatment was used to prevent hybrid-organic-siloxane-polymer (HOSP) film from photoresist stripping damage [57]. The H_2 plasma treatment can passivate the HOSP surface with active hydrogen radicals and prevent dielectric loss

originating from stripping process. The thin passivation layer formed on the surface by H_2 plasma treatment can also enhance the resistibility against moisture absorption. Therefore, the leakage current will decrease and the dielectric constant can maintain at a low value even after photoresist stripping process.

Post-deposition H_2+He plasma treatment [58] was also found to reduce the dielectric constant and increases the thermal stability of low-*k* plasma polymerized paraxylene. The reduction of the dielectric constant is attributed to the suppression of the formation of C=O and O-H groups and increase of C-H group in the low-*k* film. The thermal stability of the low-*k* films is improved because plasma bombardment and reactive hydrogen generated from the plasma increase the cross linking among film formation species.

1.4.3 NH_3 Plasma Treatment

It was shown that NH_3 Plasma treatments impact favorably on dielectric properties of non-porous HSQ low-*k* material. The treatments indeed reduce the probability of moisture absorption and suppress Cu diffusion successfully without barrier layer, while preserving the *k* value of the ILD layer. Upon plasma treatment, the mechanical properties of the low-*k* dielectric are also improved [59]. NH_3 plasma treatment provides an efficient method for improving the quality of HSQ low-*k* material. After NH_3 plasma treatment, a thin nitride film forms on HSQ without changing its dielectric constant. This film almost keeps the same dielectric constant after different plasma exposure times. With the thin nitride film, the film resistance to Cu diffusion has been improved.

This thin nitride film also improves the breakdown voltage of HSQ because the dangling bonds in HSQ are passivated by hydrogen to reduce the leakage current [60, 61]. The ultraviolet radiation and high-energy particle interaction in plasma can cause HSQ thin films decompose from cage structure to a more stable silica network. Consequently, the mechanical properties of HSQ thin film is enhanced [62].

Both chemical and physical reactions of plasma lead to a densification of the low-*k* dielectric. The densification can be confined into a few nanometers of the top layers of the dielectric films [63]. The mechanism is that NH_3 plasma treatment indeed creates N-rich cross-linked dense layer at the surface of the porous low-*k* thin film.

The plasma treatment is also effective in improving mechanical properties of low-*k* thin film. However, the study of plasma treatment effect on porous low-*k* thin film has not been investigated. Our research focus is on how to use the plasma treatment to improve the mechanical properties of porous low-*k* thin film and find out the mechanism of the effect of plasma treatment on porous low-*k* thin film.

1.5 Objective and Outlines

There is certainly a trade-off between the *k* value and the mechanical properties of the low-*k* materials, which include Young's modulus, hardness, cohesive strength, and fracture toughness [16, 64]. Typically, the hardness of porous low-*k* materials is in the order of 1.0 GPa, which is lower than the critical value, about 2 GPa, required for a low-*k* ILD film to survive packaging process [65]. The objective of this research is to develop a method that improves the mechanical strength of the porous low-*k* ILD thin

films without increasing the *k* value significantly or inducing adversary effects such as film shrinkage and plasma damage. We propose to use NH_3 plasma treatment on methyl silsesquoxane (MSQ) based porous low-*k* films to improve their mechanical properties. We conjecture that the nitridation of these films should help to enhance the mechanical strength of the films due to the incorporation of stronger Si-N bonds. Another objective of the research is to explore feasibility of using NH_3 plasma treatment to form a thin smooth dense skin layer on the porous MSQ based low-*k* films. Sealing the surface of the porous low-*k* films, the skin layer can be employed as an effective barrier to the diffusion of Cu in the porous low-*k* ILD thin films.

The mechanical properties of porous low-*k* thin films were measured by the nano-indentation method. In particular, the variation of the load/depth ratio, *P*/*h*, with the indentation depth *h* was recorded. The variation was then analyzed to determine Young's modulus and the hardness of the porous low-*k* films. The principles of nano-indentation technique are introduced in Chap. 2. Chapter 2 also introduces the principles of other experimental apparatus that was applied in the study.

In Chap. 3, the correlation between porosity and mechanical properties of porous low-*k* thin films were studied using XLK^{TM} porous low-*k* thin films provided by Dow Corning.

Chapter 4 includes two subsections. The first section presents and discusses experimental results that clearly show the improved mechanical properties of NH_3 plasma treated ZIRKON LK2200^{TM} porous low-*k* thin films as revealed by nano-indentation measurement. Detailed analysis of nano-indentation results, along

with other experimental results from transmission electron microscopy (TEM), time of flight--secondary ions sass spectrometry (TOF-SIMS), positronium annihilation lifetime spectroscopy (PALS), and Fourier transformation infrared (FTIR) spectrometry, will be presented to presented to correlated the improved mechanical properties with the plasma induced non-porous dense surface layer. In the second section, the similar improvement of mechanical properties of yet another type of porous MSQ low-*k* thin films, i.e., JSR LKD5109^{TM} porous MSQ low-*k* films, after NH_3 plasma treatment will also reported.

Chapter 5 summarizes major results of this thesis and proposes some suggestions for future work.

References

[1] R. H. Havemanm, Proc. of IEEE 89, 743 (2001).

[2] K. Beekmann, A. Wilby, K. Giles, and J. Macneil, Microelectron. Eng. 55, 73 (2001).

[3] T. W. Poon, P. S. Ho, and J. Leu, J. Phys. Chem. Solids 55, 1154 (1994).

[4] F. Caignet, D. B. Sonia, and S. Etienne, Proc. of IEEE 89, 556 (2001).

[5] S. Bothra, IEEE Trans. Electron. Devi. 40, 591 (1993).

[6] K. Y. Chou and M. J. Chen, IEEE Electron. Devi. Lett. 22, 342 (2001).

[7] W. Chang, S. M. Jang, C. H.Yu, S. C. Sun, and M. S. Liang, Proc. of Intl. Interconnect Tech. Conf., 131 (1999).

[8] K. Maex, M. R. Baklanov, D. Shamiryan, F. Lacopi, S. H. Brongersma, and Z. S. Yanovitskaya, J. Appl. Phys. 93, 8793 (2003).

[9] International Technology Roadmap for Semiconductors (Semiconductor Industry Association, San Jose, CA, 2001).

[10] T. N. Theis, J. Mater. Res. Dev. 44, 379 (2000).

[11] J. H. Golden, C. J. Hawker, and P. S. Ho, Semicond. Intl. 21, 79 (2001).

[12] P. S. Ho, J. Leu, and W. W. Lee, Low Dielectric Constant Materials for IC Application (Springer, Berlin, 2003)

[13] A. E. Kaloyeros, and E. Eisenbraun, Annu. Rev. Mater. Sci. 30, 363 (2000).

[14] J. G. Ryan, Proc. of the low-*k* Dielectric Mater. Tech. Conf., 185 (SMICON WEST, 2000).

[15] R. Goldblatt, IEEE Intl. Interconnect Tech. Conf. 263, (2000).

[16] Laura Peter, Semicond. Intl. 18, 56 (1999).

[17] W.W. Lee and P. S. Ho, MRS Bull. 22, 19 (1997).

[18] B. Zhao and M. Brongo, Mat. Res. Soc. Sypm. Proc. 565, 137 (1999).

[19] N. P. Hacker, MRS Bull. 22, 33 (1997).

[20] J. Rouquerol, D. Avnir, C. W. Fairbridge, D. H. Everett, J. H. Haynes, N. Pernicone, J. D. F. Ramsay, K. S. W. Sing, and K. K. Unger, Pure Appl. Chem. 66, 1739 (1994).

[21] Y. Xu, D. W. Zheng, Y. Tsai, K. N. Tu, B. Zhao, Q. Z. Liu, M. Brongo, C. W. Ong, C. L. Choy, G. T. Sheng, and C. H. Tung, J. Electronic Mater. 30, 309 (2001).

[22] K. Maex, M. R. Baklanov, D. Shamiryan, F. Lacopi, S. H. Brongersma, and Z. S. Yanovitskaya, J. Appl. Phys. 93, 8793 (2003).

[23] P. S. Ho, J. Leu, W. W. Lee, Low Dielectric Constant Materials for IC Applications, (Springer, New York, 2002).

[24] C. Jin, J. D. Luttmer, D. M. Smith, and T. A. Ramos, MRS Bull. 22, 39 (1997).

[25] W. Y. Shih, J. Levine, and M. Chang, Mat. Res. Soc. Sypm. Proc. 467, 479 (1999).

[26] L. A. Chow, Y. H. Xu, B. Dunn, K. N. Tu, and C. Chiang, Appl. Phys. Lett. 73, 2944 (1998).

[27] J. L. Hedrick, H. J. Cha, R. D. Miller, D. Y. Yoon, H. R. Brown, S. Srinivasan, R. D. Pietro, R. F. Cook, J. P. Hummel, D. P. Klaus, E. G. Liniger, and E. E. Simonyi, Macromolecules 30, 8512 (1997).

[28] N. P. Hacker, G. Davis, L. Figge, T. Krajewski, S. Lefferts, J. Nedbal, and R. Spear, Mat. Res. Soc. Sypm. Proc. 511, 25 (1998).

[29] A. Grill, Diamond Relat. Mater. 10, 234 (2001).

[30] A. Grill, Thin Solid Films 356, 186 (1999).

[31] H. Yang, D. J. Tweet, U. Ma, and T. Nguen, Appl. Phys. Lett. 73, 1514 (1998).

[32] J. W. Yi, Y. H. Lee, and B. Farouk, Thin Solid Films 374, 103 (2000).

[33] J. N. Sun, PhD Dissertation: Probing Porous Low-dielectric Constant Thin Films Using Positronium Annihilation Lifetime Spectroscopy, University of Michigan, 2002.

[34] C. J. Brinker and G. W. Scherer, Sol-Gel Science: The Physics and Chemistry of Sol-Gel Processing (McGraw-Hill, New York, 1990).

[35] Y. F. Lu, G. Z. Cao, R. P. Kale, S. Prabakar, G. P. Lopez, and C. J. Brinker, Chem. Mater. 11, 1223 (1999).

[36] M. Petkov, M. H. Weber, K. G. Lynn, and K. P. Rodbell, Appl. Phys. Lett. 79, 3884 (2001).

[37] S. Wolf and R. N. Tauber, Silicon Processing for the VLSI Era (Lattice, CA, 2000).

[38] A. C. Adams, VLSI Technology (McGraw-Hill, New York, 1983).

[39] S. Sivaram, Chemical Vapor Deposition (McGraw-Hill, New York, 1995).

[40] M. R. Baklanov and L. L. Vasilyeva, Mater. Sci. Forum 65, 185 (1995).

[41] M. R. Baklanov, L. L. Vasilyeva, T. A. Gavrilova, F. N. Dultsev, K. P. Mogilnikov, and L. A. Nenasheva, Thin Solid Films 171, 43 (1989).

[42] F. N. Dultsev, L. L. Vasilyeva, and L. A. Nenasheva, J. Electrochem. Soc. 145, 2569 (1998).

[43] C. Lee, E. Machlin, and H. Rathore, J. Appl. Phys. 71, 5877 (1992).

[44] E. Kolawa, J.S. Chen, J. S. Reid, P. J. Pokela, and M. A. Nicolet, J. Appl. Phys. 70, 1369 (1991).

[45] G. S. Chen and S. T. Chen, J. Appl. Phys. 87, 12, 8473 (2000).

[46] M. Lane, and R.H. Dauskardt, J. Mat. Res. 15, 203 (2000).

[47] Z. C. Wu, C. C. Wang, R. G. Wu, Y. L. Liu, P. S. Chen, Z. M. Zhu, M. C. Chen, J. F. Chen, C. I. Chang, and L. J. Chen, J. Electrochem. Soc. 146, 4290 (1999).

[48] M. Rasco, IEEE Intl. Interconnect Tech. Conf. Proc., 113 (2002).

[49] K. Mosig, Microelectron. Eng. 64, 11 (2002).

[50] J. Proost, E. Kondoh, G. Vereecke, M. Heyns, and K. Maex, J. Vac. Sci. Technol. B 16, 2019 (1998).

[51] J. Proost, M. Baklanov, K. Maex, and L. Delaey, J. Vac. Sci. Technol. B 18, 303 (2000).

[52] M. J. Loboda, C. M. Grove, and R. F. Schneider, J. Electrochem. Soc. 145, 2861 (1998).

[53] T. C. Chang, Y. S. Mor, P. T. Liu, T. M. Tsai, C. W. Chen, Y. J. Mei, F. M. Pan, W. F. Wu, and S. M. Sze, Microelectron. Eng. 60, 469 (2002).

[54] C. Y. Wang, J. Z. Zheng, Z. X. Shen, Y. Lin, and A. T. S. Wee, Thin Solid Films 397, 90 (2001).

[55] A. Satta, M. Baklanov, O. Richard, A. Vantomme, H. Bender, T. Conard, K. Maex, W. M. Li, K. E. Elers, and S. Haukka, Microelectron. Eng. 60, 59 (2002).

[56] E. Kondoh, T. Asano, A. Nakashima, and M. Komatu, J. Vac. Sci. Technol. B 18 (3), 1276 (2000).

[57] T. C. Chang, Y. S. Mor, P. T. Liu, T. M. Tsai, C. W. Chen, Y. J. Mer, F. M. Pan, W. F. Wu, and S. M. Sze, Microelectron. Eng. 60, 469 (2002).

[58] C. Q. Yong, S. Yeo, C. Shim, J. Yang, and D. Jung, J. Appl. Phys. 89, 1402 (2001).

[59] Y. Travaly, B. Eyckens, L. Carbonel, A. Rothschild, Q. T. Le, S. H. Brongersma, I. Ciofi, H. Struyf, Y. Furukawa, M. Stucchi, M. Schaekers, H. Bender, E. Rosseel, S. Vanhaelemeersch, K. Maex, L.Van Autryve, and P. Rabinzohn, Microelectron. Eng. 64, 367 (2002).

[60] K. M. Chang, I. C. Deng, S. J. Yeh, and Y. P. Tsai, Electrochem. Solid-State Lett. 2, 634 (1999).

[61] P. T. Liu, T. C. Chang, Y. L. Yang, Y. F. Cheng, and S. M. Sze, IEEE Trans. Electron. Devi. 47, 1733 (2000).

[62] T. Furusawa, D. Ryazaki, R. Yoneyama, Y. Homma, and K. Hinode, J. Electrochem. Soc. 148, F175 (2001).

[63] H. J. Lee, J. Electrochem. Soc. 148, F195 (2001).

[64] M. Fury, Solid State Tech. 42, 87 (1999).

[65] A. E. Braun, Semicond. Intl. 25, 32 (2003).

Chapter 2. Apparatus and Experiments

In this chapter, we discuss the major apparatus and the experimental procedure adopted in our study. Our investigation consists of three parts: study of the correlation between the mechanical properties of porous low-*k* thin films and their porosities, plasma treatment on porous low-*k* thin films, and the characterization of the effects of the plasma treatment. In particular, the plasma treatment was carried out in a plasma enhanced chemical vapor deposition (PECVD) system, and this technique is described in Sec. 2.1. The mechanical properties of porous low-*k* thin films with different porosity were measured by the nano-indentation technique. The nano-indentation technique was also applied to characterize the improvement of mechanical properties of porous low-*k* thin films after plasma treatment. The details of nano-indentation technique are reviewed in Sec. 2.2.

In addition to the nano-indentation method, several characterization techniques were adopted in our study to understand the physical mechanism that causes the improvement of mechanical properties of porous low-*k* thin films after plasma treatment. The characterization techniques include transmission electron microscopy (TEM), time of flight--secondary ions mass spectrometry (TOF-SIMS), and Fourier transformation infrared (FTIR) spectrometry. They are briefly introduced in Sec. 2.3. After discussing the experimental methodologies of our study, we present the details of the experimental procedures in Sec. 2.4.

2.1 Plasma Enhanced Chemical Vapor Deposition System

The plasma treatment was carried out in a plasma enhanced chemical vapor deposition system. The system can be used to generate plasma to do deposition, etching, plasma treatment and cleaning. Plasma enhanced chemical vapor deposition is commonly used to deposit dielectric layers that are used to provide electrical and physical barriers between metal interconnect layers [1]. The major component of the PECVD system is a plasma source, which provides the reactants in the gas flow with a large amount of energy for the chemical reactions to occur during the deposition. Due to the energy from the plasma, the reactions can happen at temperatures much lower than those needed when only thermal energy is provided [2]. In addition to the advantage of low deposition temperatures, PECVD also allows for tailoring the film properties for particular applications easily due to the fact that the deposition process in PECVD is further from the equilibrium state than the non-plasma CVD method. However, the non-equilibrium state can also lead to undesirable compositions or properties in the films, for example, the incorporation of byproducts or gas molecules in the film [3].

Besides deposition, plasma can also be used to do etching. There are two major approaches. In the first approach, the reactants in the gas flow are ionized by the plasma. This provides the reactants a large amount of energy to react with the material in the substrate to form a gas species that can be carried away by the gas flow. In the second approach, argon ions in the plasma bombard the substrate and dislodge atoms from the substrate. The dislodged atoms react with some species in the plasma to form another species that can be carried away by the gas flow. Both approaches can achieve

anisotropic etching by controlling the bombardment direction of the ions [2].

2.1.1 The Set-up of Orion^{TM} PECVD System

Orion^{TM} PECVD system is used in this study. It is a tabletop system with plasma deposition and plasma treatment ability. Fig. 2.1(a) shows a schematic diagram of the Orion^{TM} PECVD system and Table 2.1 summarizes the system specifications of the system. The PECVD system includes the following components [4]:

1. CVD Chamber. There is a pair of electrodes for generating an electric field to accelerate the ions to bombard the substrate in the chamber. The bottom electrode is shown in Fig. 2.1(b); it has the following three components:

(a) The lower part of the bottom electrode is used to produce a negative DC bias.

(b) An O-ring is embedded in the electrode to provide heating of the sample

(c) Water-cooling pipe to cool the chamber.

2. Vacuum System. The vacuum system is composed of a mechanical pump and a turbo pump. The pressure in the chamber is lowered to 10^{-2} torr by the mechanical pump first, and then it is further reduced to 10^{-4} torr by the turbo pump.

3. Gas Inlet. The chemical vapor deposition (CVD) reactor can have up to four process gases.

4. Radio Frequency (RF) Generator. The RF generator is used to ionize the gas in the chamber in order to produce plasma. The frequency can vary from 50 to 400 KHz to control the density of the plasma state.

5. Process Controller. The process controller controls the four gas inlets, the

pressure and the RF power. The controller is run by the software LabView® in the Windows system; thus, the controller allows the users to program the process and store the processing parameters and steps in a recipe file.

The sequence of the PECVD process is as follows. First, the sample is loaded into the chamber, and then the substrate is heated to presetted temperature by the heater. Second, the pressure in the chamber is lowered to a high vacuum level by the pumps. Afterwards, NH_3 is used to purge the chamber. Once the NH_3 flow is steady, the RF generator is turned on to activate the generation of plasma. Finally, the RF generator is turned off followed by the shut-off of the NH_3 gas. All the processes can be controlled automatically by the recipe file stored in the process controller.

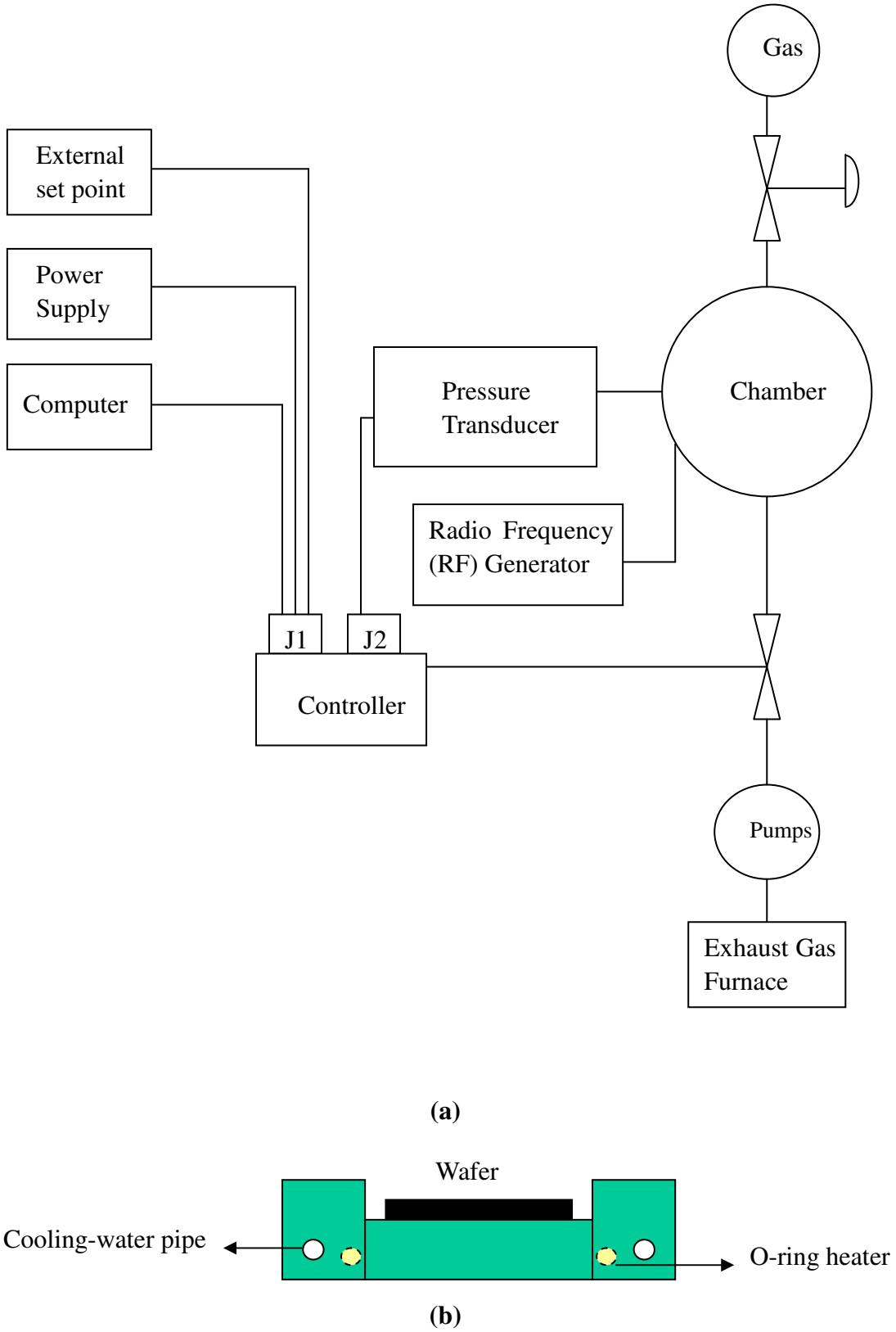

Fig. 2.1 (a) Set-up of the Orion™ PECVD system. **(b)** Cross-section of the chamber in Orion™ PECVD system.

Table 2.1 System specifications of the Orion™ PECVD system [4].

Parameters	Specifications
Size:	35″×26″ ×48″
Max RF Power:	500 watts
System Power REQ	30 amps, 280 volts, single phase
Gas Channels	Four standard, can be expanded to eight
Max Wafer Size	8″

2.1.2 The Principle of Plasma Generation

Plasmas are highly ionized gases. Plasma is typically generated by applying a high electric field to a gas to result in electrical breakdown and discharge of electrons. In general, the discharge consists of two distinct regions: dark space and luminous regions. The dark space is observed to be adjacent to two electrodes as shown in Fig. 2.2(b). The luminous region is in the center of the regime between the two electrodes. The color of the light is light purple when NH_3 is used for the plasma generation [2, 3].

The plasma is activated by many kinds of collisions. The most important collisions involving an electron and an atom are

$$\text{Elastic scattering: } e^- + A \rightarrow e^- + A \tag{2-1}$$

$$\text{Excitation: } e^- + A \rightarrow e^- + A^* \tag{2-2}$$

$$\text{Ionization: } e^- + A \rightarrow 2e^- + A^+ \tag{2-3}$$

where A^* denotes a neutral atom A in an excited state. In the elastic scattering, the electron and the atom exchange energy and momentum. For atom excitation process, the atom is collided with an electron with higher energy and momentum. Some energy of

the electron is absorbed by the atom during the collision, meaning the energy of the atom is raised to an excited state. For the atom ionization case, the atom is ionized during the collision with an electron with much higher energy and momentum. There are other collision paths for ionization, and some of them lead to different excited states [2]. Details of those collision paths and excited states can be found in Ref. 2. Once the collisions reach a steady state is reached, an electrical current flowing through the plasma as a consequence of the applied voltage. The electric current is called a DC discharge if the applied voltage is constant, and it is an RF discharge if the voltage varies with time [3]. The net current or the time-averaged RF current must be zero because the DC component of the current is blocked by the capacitor.

Plasma is a quasineutral gas consisting of charged and neutral particles exhibiting collective behavior. The term "quasineutral" means that, except for localized regions in space, the overall charge density in the plasma is zero. In other words, on average the densities of positively and negatively charged particles are equal to each other. The term "collective behavior" refers to the fact that the charged particle interact with each other via long-range coulomb forces.

Fig. 2.2(a) shows a schematic diagram of a common PECVD reactor design with the plasma being activated by the radio frequency (RF) discharges. The design consists of two parallel electrodes between which the plasma is mostly confined. One of the electrodes is often taken to be the chamber wall and is electrically grounded. The other electrode is connected to a RF-power through a blocking capacitor [2]. Fig. 2.2(b) shows the potential distribution in the chamber. The potential in the plasma is steady. There is a

potential drop at the sheath area in which the electrons are repelled from the electrodes while the ions are accelerated to the electrodes. As we all know, the light emitted from the plasma is generated when the electrons fall from higher energy level to lower energy level. Therefore, the sheath area is dark because there are very few electrons in this area.

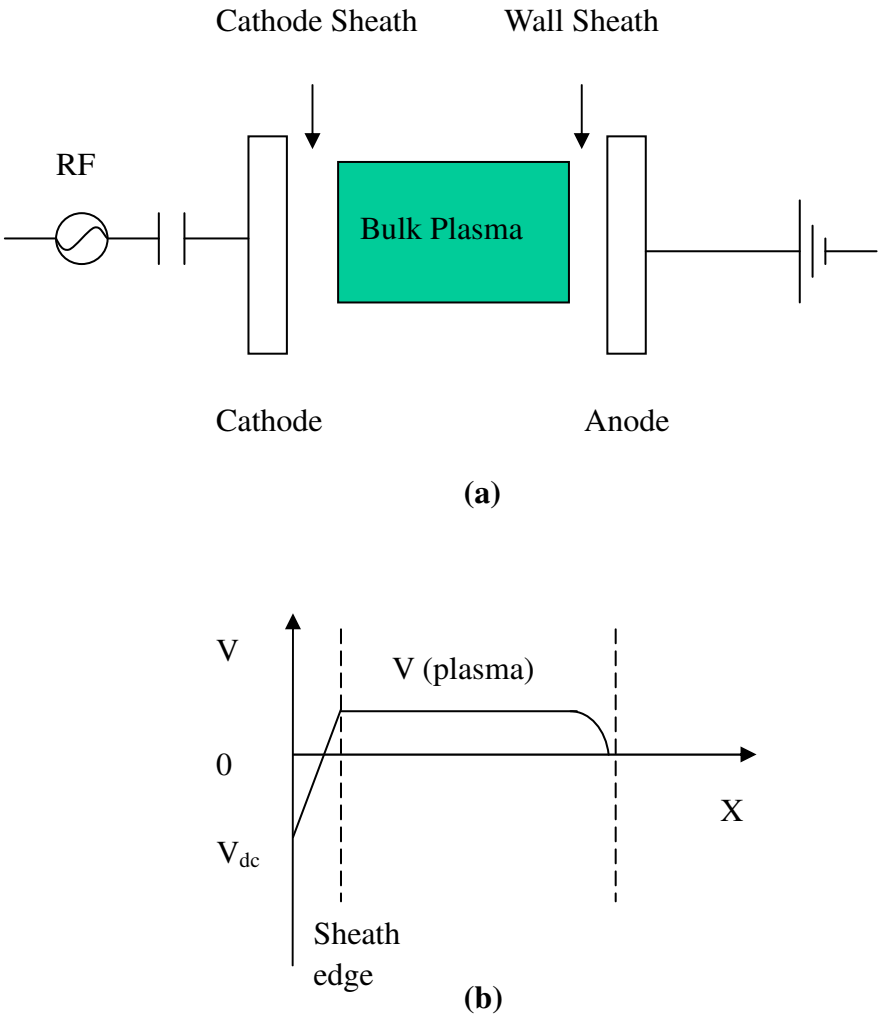

Fig. 2.2 (a) The geometry of parallel electrode structure. **(b)** The potential distribution of plasma in the chamber.

2.2 Nano-indentation Test

The nano-indentation is a reliable and convenient method for determining the mechanical strength of materials. The method is particularly useful in the situations when fabricating tension test samples of the materials is difficult, for example in the case of the film-substrate systems.

2.2.1 Introduction to Nano-indentation System

Fig. 2.3 shows a schematic diagram of the hardware of the MTS Nano-Indenter XP^{TM}, the equipment employed in our indentation tests for measuring the mechanical properties of the dielectric films. The top of the equipment is a coil magnet assembly, which controls the force imposed on the indenter tip by applying a current through the coil. Below the magnet assembly is a capacitance gauge for measuring the displacement of the diamond indenter tip. The diamond indenter tip has a pyramid shape with an angle of 89 degrees. Under the indenter tip, it is the X-Y table on which the sample is fixed. The resolution of the loading and the displacement of the MST nano-indenter and the maximum load and indentation depth allowed by the equipment are summarized in Table 2.2 [5, 6]. The resolution of the measured data, however, is also affected by the external conditions surrounding the equipment. Therefore, the laboratory conditions, such as vibration, noise, humidity, air current and temperature must be well controlled.

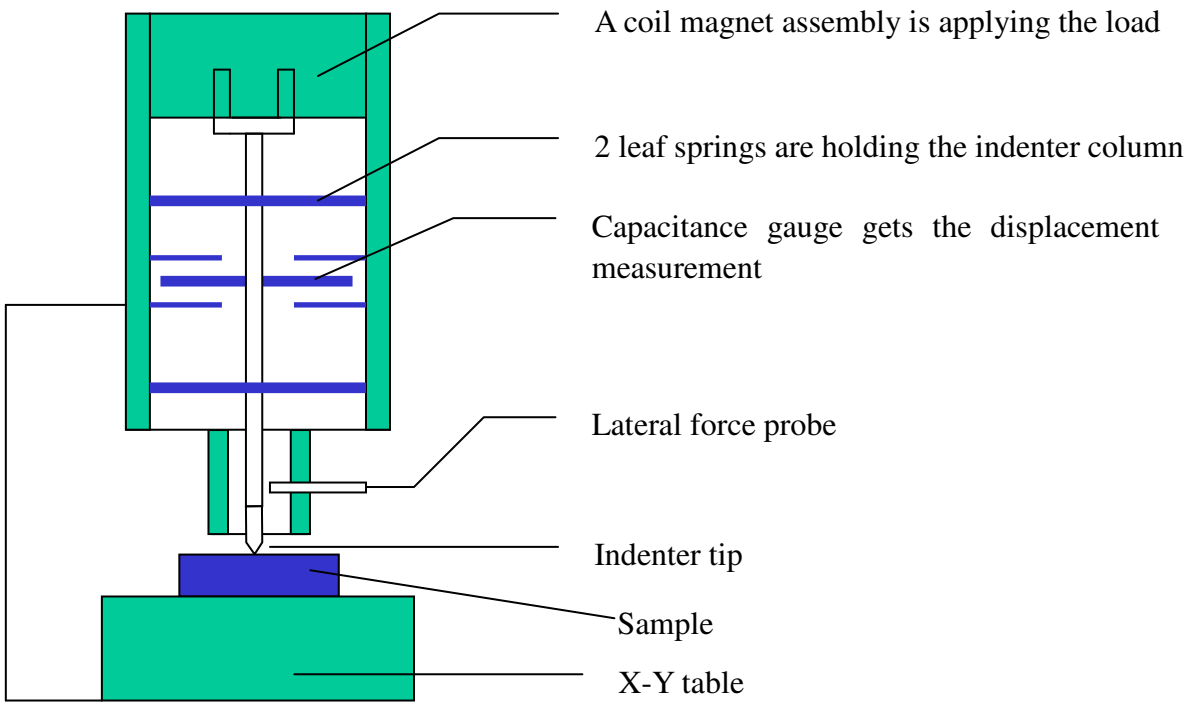

Fig. 2.3 Schematic diagram of nano-indentation (MTS Corporation).

Table 2.2 MTS nano indenter XP^{TM} specifications.

Parameters	Specifications
Displacement resolution	<0.01 nm
Maximum indentation depth	500 酸
Maximum load	500 mN
Load resolution	50 nN
Load resolution	50 nN
Position control	Remote with mouse (motorized in x-, y-, and z-directions). Fully automated during experiments

The nano-indentation test procedure consists of three segments: loading, holding, and unloading. A schematic diagram of the loading vs. indentation depth during the nano-indentation test is shown in Fig. 2.4. From point A to point B is the loading segment; from point B to point C is the holding segment; and from point C to point D is

the unloading segment [7, 8]. *S* represents the contact stiffness while h_c is the contact depth.

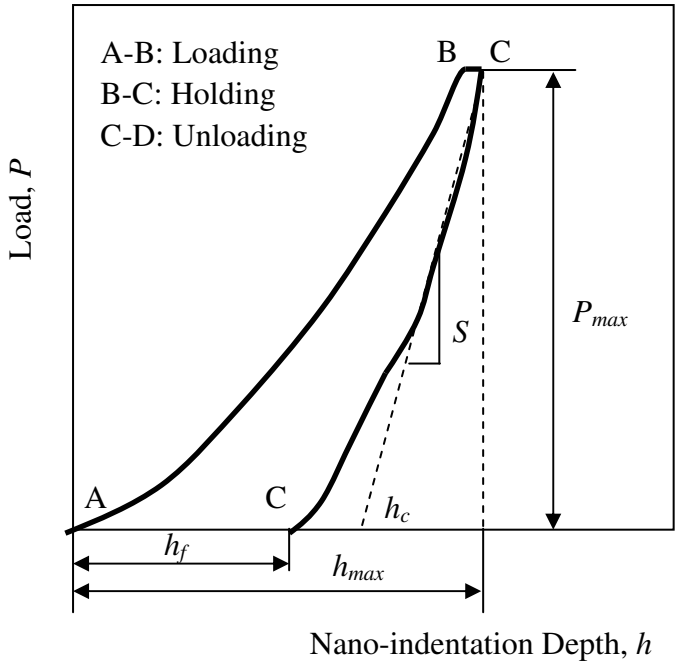

Fig. 2.4 Schematic representation of load versus displacement during nano-indentation.

The nano-indentation, in essence, is similar to other hardness measurement methods, such as Brinell hardness test [9]. All of the methods adopt a hard tip to make a permanent impression on the surface of the sample. The ratio between the applied force and the area of the impression gives the hardness of the material. In spite of the similarity, there are distinguished differences between nano-indentation test and the other hardness tests. The first difference is that the indentation depth in the nano-indentation test is in the nanometer scale, while the indentation depth in the other hardness tests is of the order of magnitude of 10^{-6} m or more. The second difference is that the loading and the indentation depth are recorded during the process. Because of the recorded data of loading and indentation depth, the nano-indentation method can provide more

information of the mechanical properties of the material.

2.2.2 Application of Nano-indentation in Measuring Mechanical Properties of Low-*k* Materials

The nano-indentation is a widely used approach for the determination of the mechanical properties of thin films [10-12] besides other techniques such as the micro-tensile testing of freestanding films, the wafer curvature method, and the beam bending technique [13-15]. In this project, the nano-indentation was used to determine how Young's modulus and the hardness of porous low-*k* thin films are affected by plasma treatments.

Young's modulus and the hardness of the thin films were measured by a Nano Indenter XP^{TM} (MTS Cooperation, Nano Instruments Innovation Center, TN, USA) with a continuous stiffness measurement (CSM) mode at a constant strain rate. The strain rate in nano-indentation test is defined as the penetration rate of indenter divided by the indentation depth. In the CSM mode, an alternating force is superimposed on the nominal applied force. This oscillating force with known phase and amplitude interacts with the sample, which responds with a displacement phase and amplitude characteristic of the stiffness and damping of the contact with the indenter. The stiffness data of CSM were recorded with load and displacement data. Thus, the Young's modulus and hardness can be calculated at every data point during the indentation experiment. Therefore, the Young's modulus and hardness can be determined as functions of indentation penetration depth with a single indentation load/unload cycle [16].

The procedures adopted in our nano-indentation experiments can be described as follows. First, the indenter approached and contacted the sample surface; the indenter then penetrated into the sample at a constant strain rate of 0.05 (s^{-1}) to a pre-defined maximum depth; the load at this maximum depth was held for 10 seconds; afterwards, the indenter was withdrawn from the sample at the same rate as loading, but not completely. The indenter was held in contact with the sample surface at 10% of the maximum load for 60 s before it withdraws from the sample completely.

From the load-displacement curve, Young's modulus E and hardness H are determined by two equations below,

$$\frac{E}{1-\nu^2} = \frac{\sqrt{\pi}}{2}\frac{1}{\sqrt{A_{\max}}}\frac{\mathrm{d}P}{\mathrm{d}h} \tag{2-4}$$

and

$$H = \frac{P_{\max}}{A_{\max}} \tag{2-5}$$

where ν is Poisson's ratio, dP/dh is the slope of the indentation unloading curve at the maximum load, $P_{\max}$ is the maximum indentation load, and $A_{\max}$ is the maximum contact area under the maximum indentation load. Generally, Poisson's ratio is preset to be 0.3 because it is known that Poisson's ratio has little effect on Young's modulus and the hardness determined by the nano-indentation technique [16].

Young's modulus and the hardness of thin films measured by indentation are affected by the mechanical properties of the substrate. It is necessary to separate the substrate effects from the measured properties. The following Eq. (2-6) is based on the assumption that the sample is a homogeneous material [17]

$$P=Ch^2 \tag{2-6}$$

where P is the indentation load, h is the indentation depth corresponding to that load, and C is a constant which depends on the properties of the materials such as Young's modulus, yielding stress and strain hardening. The assumption is valid for the case of thin film if the film thickness is sufficiently large so that the effect of the substrate can be ignored. Eq. (2-6) can be transformed to get

$$P/h=Ch \tag{2-7}$$

The relation suggests that if the film in the sample is sufficiently thick, P/h increases with h linearly. On the contrary, if the sample contains a thin film that the substrate effect is significant, P/h cannot be described as a linear function of the indentation depth h. This demonstrates that the change of the slope of the P/h versus h curves would indicate the influence of the substrate on the measured mechanical properties of thin films. In our analysis, the linear range of P/h versus h was used to determine the range in which the measured Young's modulus and hardness are the real value of the thin film. Furthermore, the change of slope of P/h versus h curve can be used to separate the impact of the underlying thin films to get the range in which the measured Young's modulus and hardness are the real value of the surface thin film.

2.3 Other Experimental Apparatus

In order to understand the physical mechanism that causes the improvement of mechanical properties of porous low-k thin film after plasma treatment, several characterization techniques were also employed in this study. They are briefly

introduced in the following subsections.

2.3.1 Fourier Transformation Infrared Spectrometry

Fig. 2.5 depicts the basic set-up of transmission mode of Fourier transformation infrared (FTIR) spectrometry, a technique adopted in our project to analyze the change of the chemical composition in the film. In the transmission mode, the infrared waves are generated from a source and pass through the sample. Some of the waves are absorbed by the sample and others transmit through the sample. Detecting and analyzing the waves transmitting through the sample determines the functional groups in the sample [18]. In our project, the FTIR analyses were carried out by Spectrum 2000 FTIR and the wave number of the infrared light were in the range from 400 to 4000 cm^{-1}.

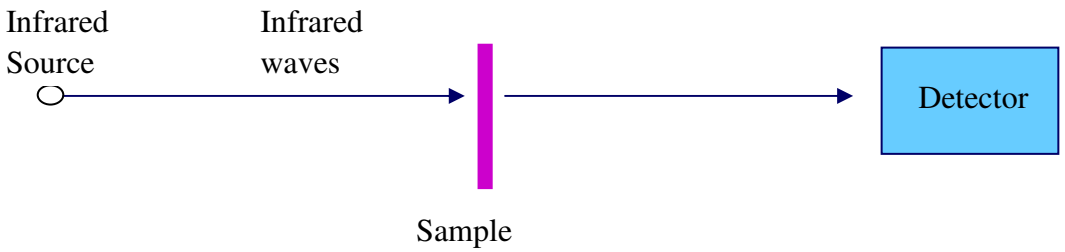

Fig. 2.5 Schematic diagram of Fourier transformation infrared (FTIR) spectrometer.

2.3.2 Atomic Force Microscope

Fig. 2.6 shows the schematic diagram of atomic force microscope (AFM). The diamond tip contacts the sample surface directly, with the interatomic Van der Waals forces providing the interaction mechanism. The tip is moved laterally on the sample surface under the condition that the force is maintained to be a constant. This is achieved

by adjusting the vertical position of the tip. The cantilever's vertical movement is detected by a laser, which is reflected from the back of the reflective AFM cantilever and second-reflected onto a position-sensitive detector through a mirror. Therefore, the variation of the vertical position on the surface gives the morphology of the sample.

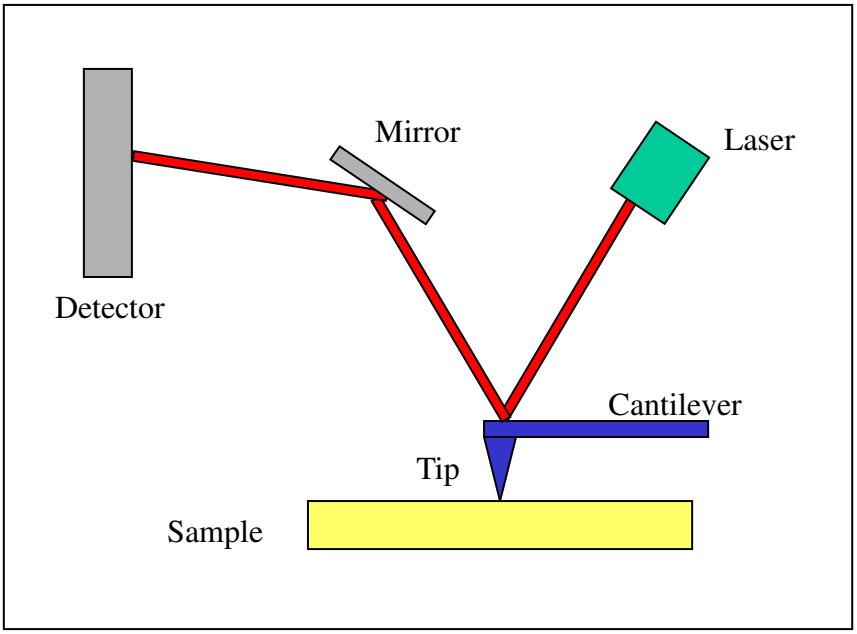

Fig. 2.6 Schematic diagram of AFM.

There are three modes of AFM: contact mode, non-contact mode, and tapping mode. In the contact mode, the small contact areas between tip and the sample surface result in high stresses that can damage either the sample or the tip or both. For non-contact mode, the lateral resolution is limited by the tip-sample separation and is normally lower than that in either contact mode or tapping mode. Tapping mode overcomes problems associated with friction, adhesion and electrostatic forces; thus, the mode can achieve high resolution without inducing destructive frictional forces on the tip and sample [19]. Because of these advantages, the tapping mode was used to measure

the surface image of porous low-*k* thin films. In our study, the surface roughness of porous low-*k* thin film is characterized by Digital Instrument Nano IIIA AFM.

2.3.3 Transmission Electron Microscopy

Fig. 2.7 shows simple schematic diagram of transmission electron microscopy (TEM). In the TEM analyses, electrons generated by the electron gun pass through the sample and are collected by the detector behind the sample. An electron passing through a solid may be scattered once (single scattering), several times (plural scattering), or many times (multiple scattering). Each scattering event might be elastic or inelastic. The scattered electron is most likely to be forward scattered but there is a small chance that it will be backscattered [20]. The transmitted electrons were collected by the electron detector and then the image can be obtained by the density of the electrons.

In our study, TEM is used to obtain the cross-section image of the dielectric film. This is done by Philip CM300 TEM and the magnification of the microscope was set at 30,000 times for low magnification observation and 200,000 times for high magnification observation.

2.3.4 Time of Flight--Secondary Ions Mass Spectrometry

Fig. 2.8 shows the basic theory of secondary ions mass spectrometry (SIMS) analysis. The SIMS measurement is based on the following physical phenomenon. When the sample is sputtered by primary ions with a few keVs energy, a fraction of the particles emitted from the target is ionized and they are called secondary ions. The

secondary ions can be accelerated in an electric field and collected. The mass of the secondary ions can be determined; consequently, the species of the ions can be identified and the number of the species can be counted. This provides the information about the elemental, isotopic and molecular composition of its uppermost atomic layer and the concentration of the elements in the layer [21]. By sputtering away the surface of the sample at a constant rate, a depth profile of the chemical species can be obtained [1]. SIMS analysis was adopted in our project to characterize the chemical compositions and their depth profiles of porous low-*k* thin films and it was carried out in ION TOF SIMS IV in IMRE.

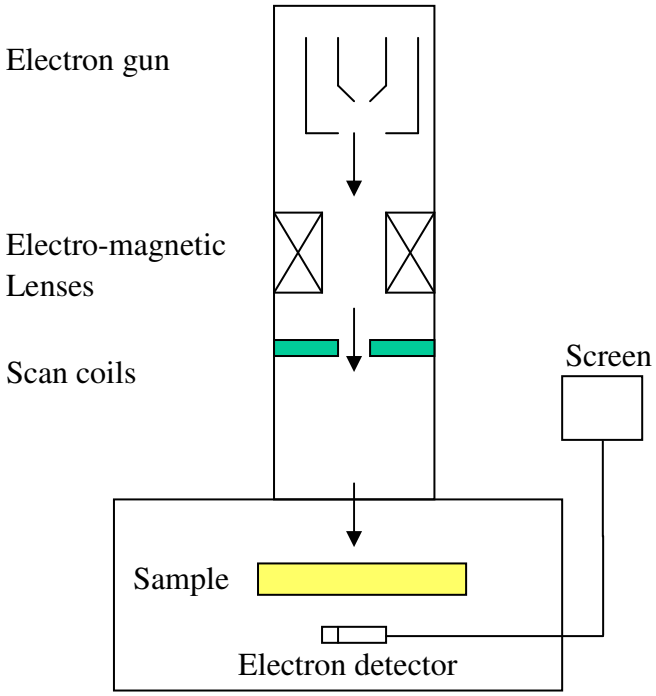

Fig. 2.7 Simple schematic diagram of TEM.

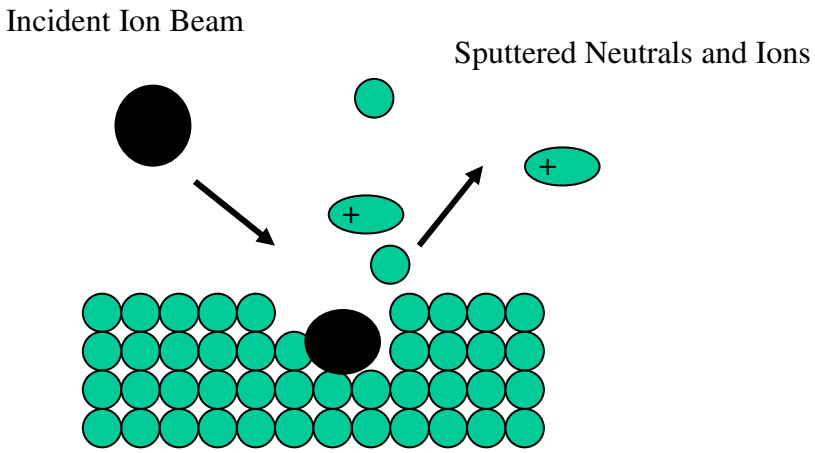

Fig. 2.8 Schematic diagram of SIMS characterization.

2.4 Experiments

2.4.1 Samples

In our study, three kinds of porous low-*k* thin films were used: XLK^{TM} porous low-*k* thin films with different porosity provided by Dow Coring, LK2200^{TM} porous low-*k* thin films provided by ZIRKON, and LKD5109^{TM} porous low-*k* thin film provided by JSR.

XLK^{TM} films are porous low-*k* films based on Dow Corning's production-proven hydrogen silsesquioxane (HSQ) spin-on resin. With the introduction of pores, the dielectric constant *k* of the film can be as low as 2.0. The thickness of the XLK^{TM} porous low-*k* thin films is around 1 酸

ZIRKON LK2200^{TM} film is MSQ-based porous low-*k* thin film. The *k* value of the film is 2.2 and the thickness of the thin film is 1 酸 The pores in the film are tubular

shaped. The average pore size is 2.7 nm and percolation length is 300 nm as revealed by positronium annihilation lifetime spectroscopy measurement, which was carried out by our collaborators in the University of Michigan.

LKD5109^{TM} porous low-*k* thin film is also MSQ-based material but with different pore interconnectivity. The thickness of LKD5109^{TM} porous low-*k* thin film is around 0.8 酸. The film has the same *k* value as ZIRKON LK2200^{TM} film. Similar to ZIRKON LK2200^{TM} films, the pores in LKD5109^{TM} porous low-*k* thin film are tubular shaped with an average pore diameter of 2.7 nm. However, unlike the ZIRKONLK2200^{TM} films, the pores in LKD5109^{TM} film are fully interconnected with a percolation length larger than film thickness. Table 2.3 summarizes the properties of the two kind thin films. All the samples were blown with N_2 to clean the surface and cut into small pieces of 1cm by 1cm.

Table 2.3 Comparison between properties of ZIRKON LK2200^{TM} and JSR LKD5109^{TM}.

Film	Dielectric Constant (k)	Pore Diameter (nm)	Thin Film Thickness(A)	Percolation Length (A)
ZIRKON LK2200^{TM}	2.2	3.8 ± 0.2	10000	3000
JSR LKD5109^{TM}	2.2	4.2 ± 0.3	8000	>8000

2.4.2 Study of Correlation between Porosity of Porous Low-*k* Thin Film and Its Mechanical Properties

The XLK^{TM} films are used to study the correlation between porosity of porous low-*k* thin films and their mechanical properties. The porosity of XLK^{TM} thin film was calculated by Eq. (3-1), which will be discussed in detail in Chap. 3. The mechanical

properties were evaluated by nano-indentation technique. Before nano-indentation test, it was necessary to examine the surface roughness of the film to ensure that the roughness was sufficiently lower than the indentation depth to avoid large error in the nano-indentation results. Afterwards, the mechanical properties were studied by nano-indentation technique. The details of nano-indentation experiments and how to analyze the loading curve to get Young's modulus and hardness have already been explained in the Sec. 2.2. It is found that high porosity leads to lower mechanical strength in our study and the correlation can be established by empirical equation, which will be discussed in detail with the results in Chap. 3.

2.4.3 NH_3 Plasma Treatment

ZIRKON LK2200^{TM} porous thin films were treated in Orion^{TM} plasma enhanced chemical vapor deposition system to improve the mechanical strength of the films. After the samples were loaded into the chamber, the chamber was pump to high vacuum by the two-stage pump system. Then, NH_3 plasma was generated by a radio frequency generator with NH_3 gas flowing at a fixed rate of 100 standard cubic centimeters per minute (sccm) under 300 mtorr working pressure. The substrate temperature during the plasma treatment was kept at 300 蚓while the RF power was 150 W. Porous low -*k* thin films were treated in the NH_3 plasma with different exposure times: 3 seconds, 10 seconds, 30 seconds, and 60 seconds.

2.4.4 Characterization of the Improvement of Mechanical Properties of Porous Low-*k* Thin Film after NH_3 Plasma Treatment

The effect of NH_3 plasma treatment on the mechanical properties of the low-*k* films was investigated by the nano-indentation. The parameters adopted in the nano-indentation method were identical to those used for the as-received samples. The result showed higher young's modulus and hardness near the surface.

In order to identify the mechanism that led to the improvement of the mechanical strength after the NH_3 plasma treatment, SIMS and FTIR were first conducted. The SIMS result showed that the C-depletion and N-incorporation layer formed at the surface of the porous low-*k* thin film. The peak intensity of transmitted infrared did not show observable change after plasma treatment. The results derived from the SIMS and FTIR suggest that a dense hard layer formed on the surface of porous low-*k* thin film.

To further confirm the formation of porous low-*k* thin film, TEM was employed to observe the cross section image of the porous low-*k* thin film. The samples were cut into small pieces. Then they underwent several grinding and polishing steps until their thickness were reduced to around 30 micrometers. Finally, the samples were milled by broad-beam ion milling until it is transparent to electrons. During the ion milling process, the sample was frequently moved to an optical microscope and inspected. After the sample preparation was accomplished, it was observed under TEM. The cross section image obtained by TEM confirmed our speculation that a dense hard layer formed on the surface of the porous low-*k* thin film.

The significant improvement of the mechanical strength of the ZIRKON

LK2200^{TM} porous low-*k* thin films due to the NH_3 plasma treatment suggests that the treatment can be applied to other MSQ porous thin films. This application was explored by considering the case of and LKD5109^{TM} porous low-*k* thin films. The experimental procedure is similar to that of ZIRKON LK2200^{TM} porous low-*k* thin films. The result shows that same trend of improvement of mechanical properties of ZIRKON LK2200^{TM} porous low-*k* thin films after plasma treatment. This confirms that the plasma treatment method is an effective method for improving the mechanical properties of porous low-*k* thin film.

References

[1] J. D. Plummer, M. D. Deal, and P. B. Griffin, Silicon VLSI Technology (Prentice Hall, Upper Saddle River, NJ, 2000).

[2] B. Chapman, Glow Discharge Processes: Sputtering and Plasma Etching (Wiley, New York, 1980).

[3] J. P. Schaffer, A. Saxena, S. D. Antolovich, T. H. Sanders, S. B. Warner, The Science and Design of Engineering Materials (McGraw-Hill, San Francisco, 1999)

[4] Orion PECVD user manual (Trion Company, 2000).

[5] TestWorks® Software Handbook for Nano-indentation Systems (MTS Corporation, 2001).

[6] Nanoindenter Software Handbook (Knoxville, TN, Nano Instruments INC., 1992).

[7] W. C. Oliver and G. M. Pharr, J. Mater. Res. 7, 1564 (1992).

[8] M. F. Doerner, and W. D. Nix, J. Mater. Res. 1, 601 (1986).

[9] F. R. Brotzen, Int. Mater. Rev. 39, 24 (1994).

[10] H. Ishikawa, S. Fudetani, and M. Hirohashi, Appl. Surf. Sci. 178, 56 (2001).

[11] U. Beck, D. T. Smith, G. Reiners, and S. J. Dapkunas, Thin Solid Films 332, 164 (1998).

[12] X. Chudoba, N. Schwarzer, F. Richter, and U. Beck, Thin Solid Films 377, 366 (2000).

[13] M. Morgen, E. T. Ryan, J. H. Zhao, C. Hu, and T. Cho, P. S. Ho, Annu. Rev. Mater. Sci. 30, 645 (2000).

[14] J. H. Zhao, T. Ryan, and P. S. Ho, J. Appl. Phys. 85, 6421 (1999).

[15] J. H. Zhao, I. Malik, T. Ryan, E. T. Ogawa, and P. S. Ho, Appl. Phys. Lett. 74, 944 (1999).

[16] L. Shen, K. Y. Zeng, Y. H. Wang, B. Narayanan, and R. Kumar, Microelectron. Eng. 70, 115 (2003).

[17] P. L. Larsson, A. E. Giannakopoulos, E. Soderlund, and R. Vestergaard, Int. J. Solid Structures 33, 221 (1996).

[18] W. Neagle and D. R. Randell, Surface Analysis Techniques and Applications (Royal Society of Chemistry, Cambridge, 1990).

[19] MultiMode^{TM} SPM Instruction Manual (Digital Instrument Veeco Metrology Group, 1997).

[20] D. B. Williams and C. B. Carter, Transmission Electron Microscopy—Basics (Plenum Press, New York, 1996).

[21] Z. B. Alfassi, Non-destructive Elemental Analysis (Blackwell Science, Nalden MA, 2001).

Chapter 3. Correlation between Porosity and Mechanical Properties of Porous Low-*k* Thin Films

The dielectric constant of a thin film is related to its porosity. Generally, a thin film with higher porosity has a lower dielectric constant, a desirable property for dielectric films used in the semiconductor manufacturing. However, higher porosity leads to weaker mechanical properties. Consequently, porous low-*k* thin films will cause many challenges in CMP and packaging [1, 2]. Therefore, it is of high importance to investigate the correlation between porosity and mechanical properties.

This chapter illustrates the effects of the film porosity on Young's modulus and hardness of XLK^{TM} porous low-*k* thin films. The porosities of the films were calculated from the dielectric constant value by Eq. (3-1). Young's modulus and hardness of porous low-*k* thin films were obtained through analyzing the loading (*P*) versus indentation depth (*h*) curve recorded during nano-indentation measurement. The details of the nano-indentation technique are presented in Chap. 2. The focus of our analyses in this chapter was on the case of the XLK^{TM} low-*k* film. The purpose of the analyses is to demonstrate the capability of the nano-indentation technique in determining the effects of the film porosity on the mechanical properties of the film.

Before we proceed to discuss the mechanical properties of the porous films in the remaining of the chapter, we first briefly discuss how to determine the porosity of the films. The porosity of the XLK^{TM} porous low-*k* thin film can be calculated by the

following equation [3]

$$\ln k = x \ln k_1 + (1-x) \ln k_2 \tag{3-1}$$

where k is the dielectric constant of the porous low-k thin film, k_1 is the dielectric constant of air, k_2 is the dielectric constant of the base material, and x is the porosity.

Three different XLK^{TM} films were used in our study; the k values of the three films are 2.5, 2.2, and 2.0. According to Eq. (3-1), the porosity of the films can be calculated to 7.7%, 20.6%, and 30.1%, respectively. The result is summarized in Table 3.1. For convenience, the film with k = 2.0, 2.2, and 2.5 are named after the corresponding dielectric constant. For example, the XLK2.0 film refers to the XLK^{TM} film with k = 2.0

Table 3.1 Porosity of XLK^{TM} porous low-k thin films.

XLK^{TM} Thin Films	Film Dielectric Constant	Porosity (%)
XLK2.0	2.0	30.1
XLK2.2	2.2	20.6
XLK2.5	2.5	7.7

3.1 Surface Roughness

Before performing nano-indentation, the surface roughness of the films was examined to ensure that the roughness was sufficiently lower than the indentation depth to avoid large error in the nano-indentation results. Figs. 3.1(a), 3.1(b), and 3.1(c), respectively, depict the AFM surface scan results of the three XLK^{TM} films with the porosity being 7.7%, 20.6%, and 30.1%. The RMS (root-mean-square) surface roughness of the three films was found to be 4.08 nm, 5.12 nm, and 5.96 nm, respectively. The surface roughness of the three films are much less than the typical

indentation depth, which is about 400 nm; thus, the surface roughness would not cause problems in our nano-indentation experiments

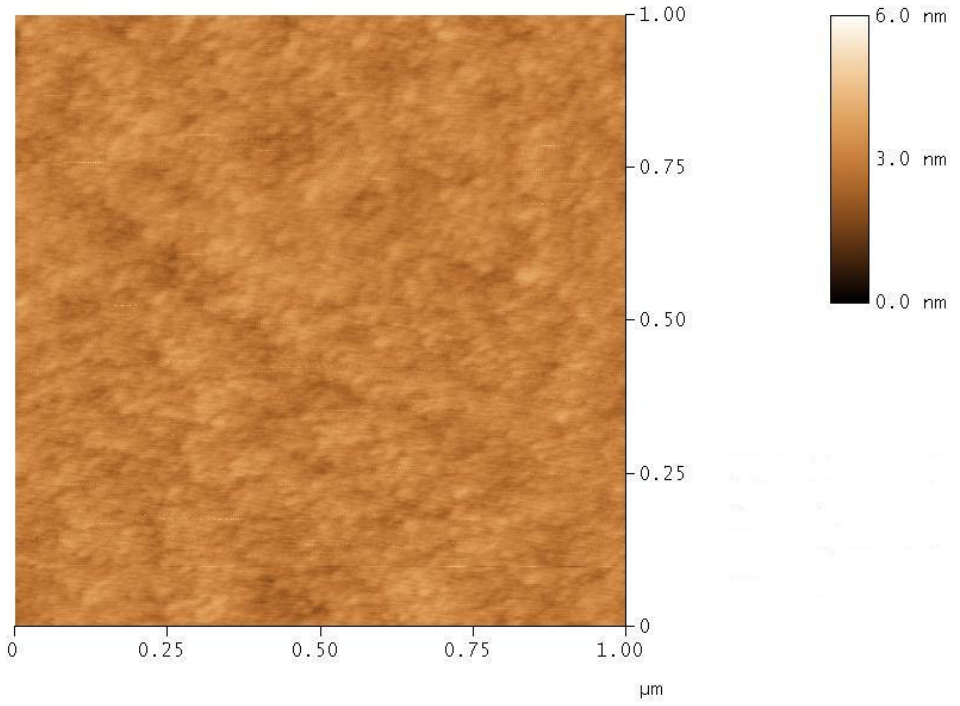

(a)

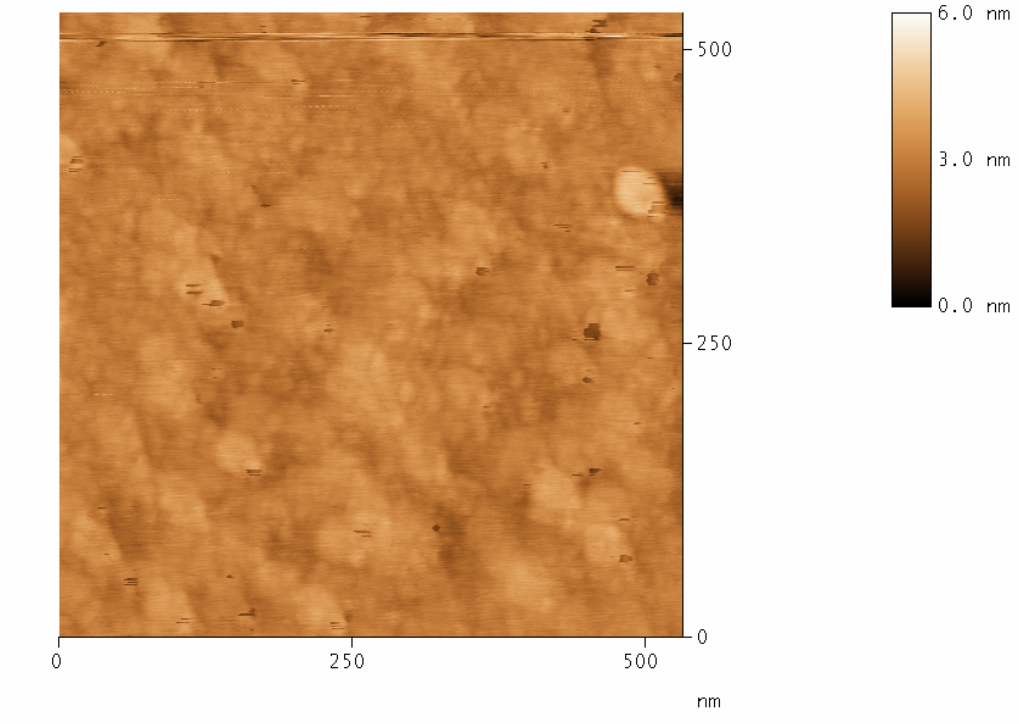

(b)

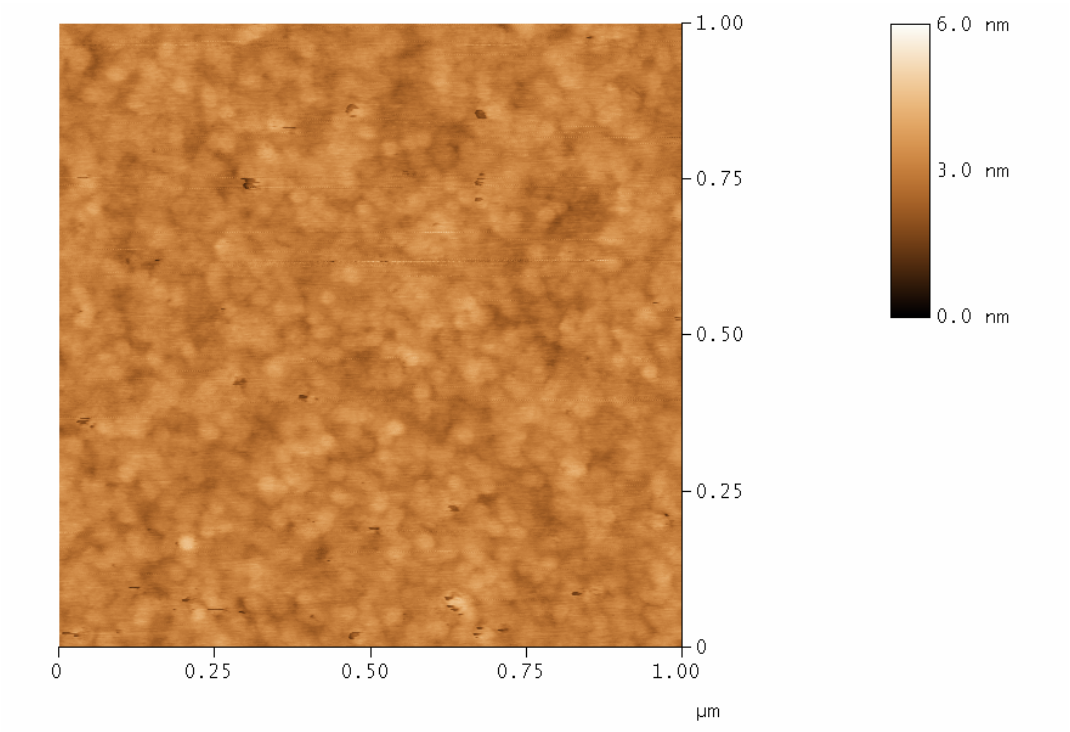

(c)

Fig. 3.1 The AFM surface scan result of **(a)** XLK2.5, **(b)** XLK2.2, and **(c)** XLK2.0 films. The porosities of the films are 7.3, 20.6, and 30.1%, respectively.

3.2 *P/h* versus Indentation Depth Curves Analysis

After the surface roughness was evaluated, the XLK^{TM} porous low-*k* thin films were tested by nano-indentation. Fig. 3.2 compares the *P/h* (load over indentation depth) versus indentation depth curves of the three thin films. The curves are analyzed by the procedure discussed in Sec. 2.2 to determine the variation of $C = d^2P/dh^2$ with the indentation depth. The quantity *C* is a material property of the low-*k* film which depends on the porosity of the film material, but independent of the properties of the substrate. The quantity *C* is termed the film indentation resistance in this thesis. For all of the three cases shown in Fig. 3.2, the indentation resistance is a constant for shallow indentation

depth. Beyond this range, the resistance *C* increases sharply with *h* because of the substrate effect.

Comparing the results of the three films indicates that the range of the indentation depth with a constant indentation resistance *C* is shorter for the film with a higher porosity. Thin film with higher porosity is softer; thus, the substrate effect appears earlier. This explains why the indentation depth range of constant *C* is smaller in films with higher porosity.

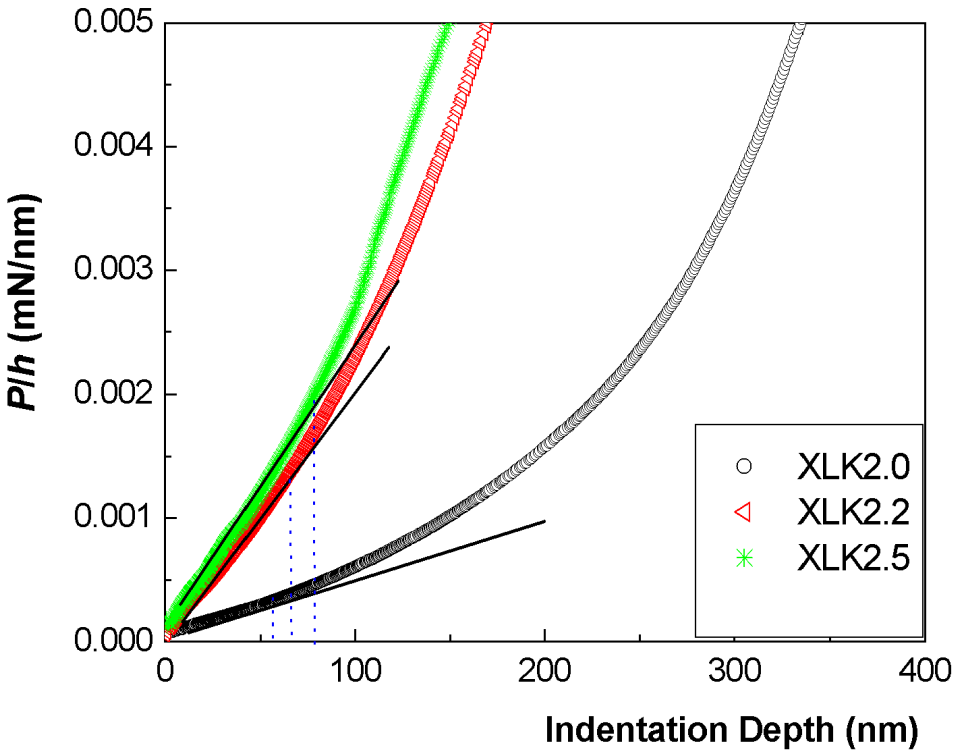

Fig. 3.2 *P*/*h* versus indentation depth curves for the XLK2.0, XLK2.2, and XLK2.5 films. The porosities of the films are 7.3, 20.6, and 30.1%, respectively.

The three cases in Fig. 3.2 suggest that the film indentation resistance *C* is higher when the porosity is lower. The statistical significance of this result is further investigated by carrying out ten indentation tests for each film to obtain the average

value and the standard deviation of *C*. The results, depicted in Fig. 3.3, indicate the standard deviation is much smaller than the difference of *C* among the three films. This demonstrates that the differences of *C* among the three films are statistically significant. The film indentation resistance *C* decreases with the porosity.

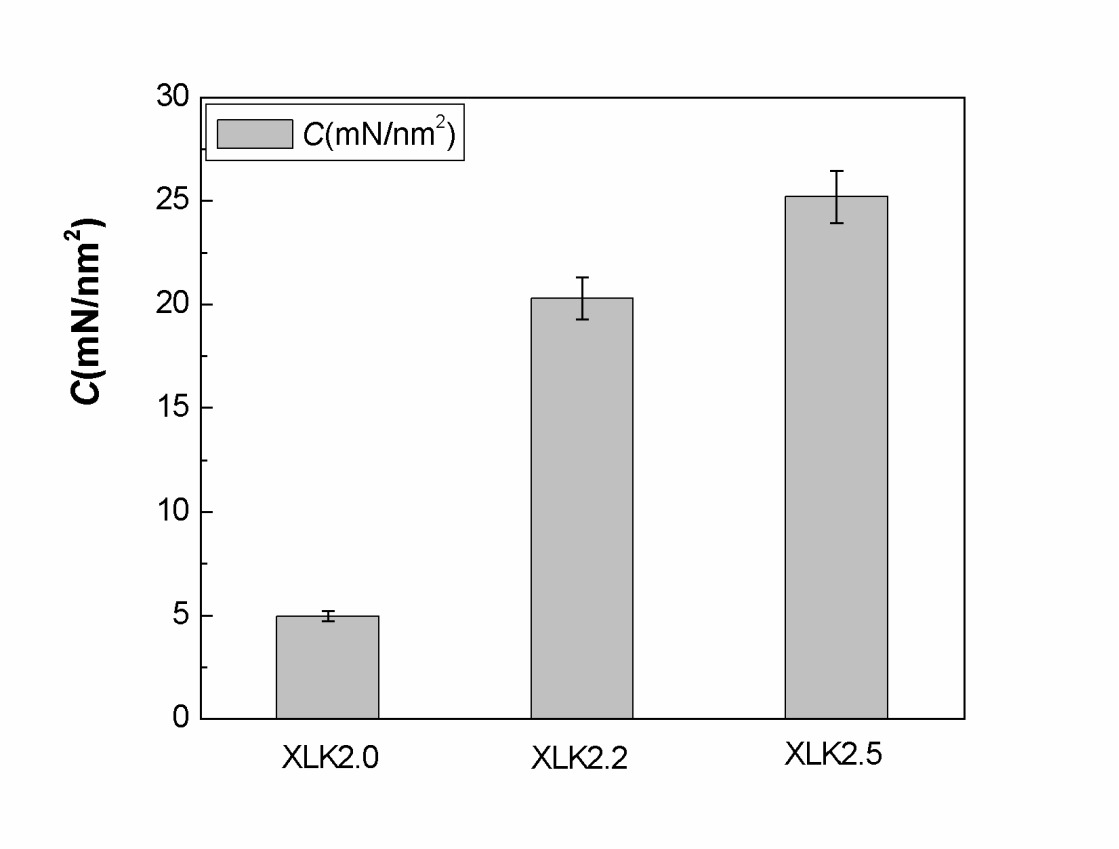

Fig. 3.3 Nano-indentation resistance (*C*) for XLK^{TM} porous low-*k* thin films with different dielectric constant.

3.3 Young's Modulus and Hardness

Fig. 3.4(a) depicts Young's modulus *E* of XLK^{TM} porous low-*k* thin films measured by the nano-indentation method. The measured Young's modulus *E* varies with the indentation depth. The variation of Young's modulus with *h* can be separated into three regimes. In the first regime, the measured values of Young's modulus decrease with the increasing indentation depth because of the surface effect and other system errors in the

nano-indenter. In the second regime, the measured E is a constant, and in the third regime, the measured values of Young's modulus increase because of the substrate effect. Similar trends are also found in Fig. 3.4(b), which plots the variation of the hardness measured by the nano-indentation method.

The second regime in which E is a constant and the effects of the surface roughness and substrates are insignificant can be adopted to determine Young's modulus of the porous films. To visualize the specific second regime, the variation of E with h is redrawn in Fig. 3.5 with the focus on the indentation depth range h is less than 100 nm. The result clearly indicates that the second regime is in the range between 20 and 60 nm for this particular case. The second regime is further confirmed by the linear range of the P/h versus indentation depth curve plotting in the same figure, which shows the value of nano-indentation resistance, $C = d^2P/dh^2$, is also a constant (C = 4.96E-6) when h is less than 60 nm. Once the second regime is identified, Young's modulus of the film is determined by taking the average of the measured E in the regime. The second regime changes slightly in each case; thus, the regime has to be checked for every test. The analysis procedure is also applied to determine the hardness of the film.

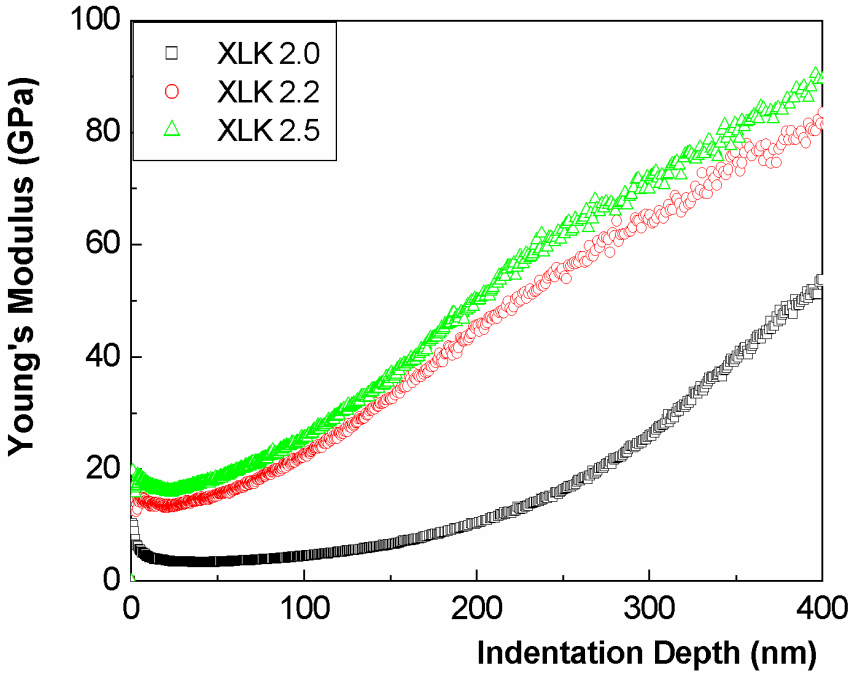

(a)

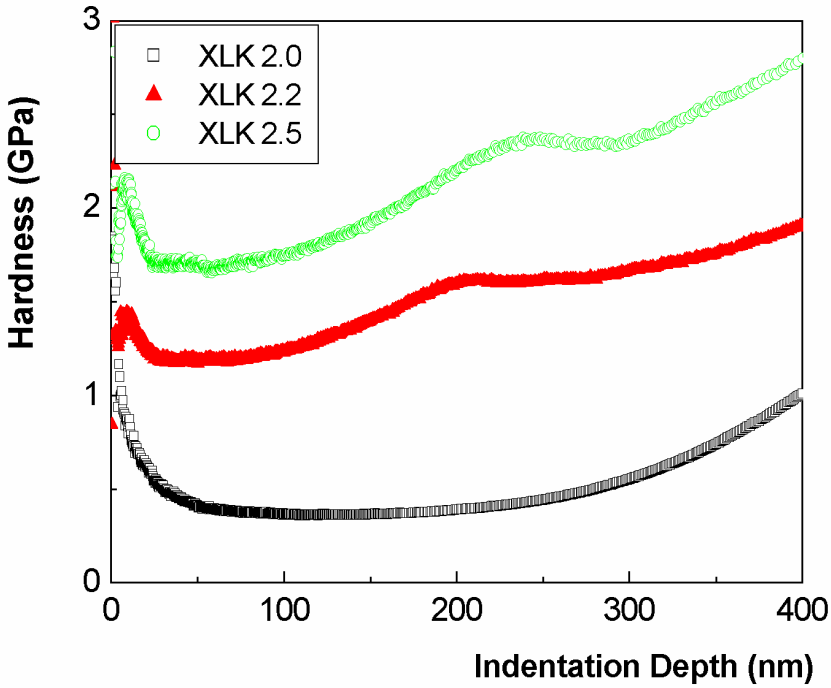

(b)

Fig. 3.4 (a) Young's Modulus of XLK^{TM} porous low-*k* thin films versus indentation depth. **(b)** Hardness of XLK^{TM} porous low-*k* thin films versus indentation depth.

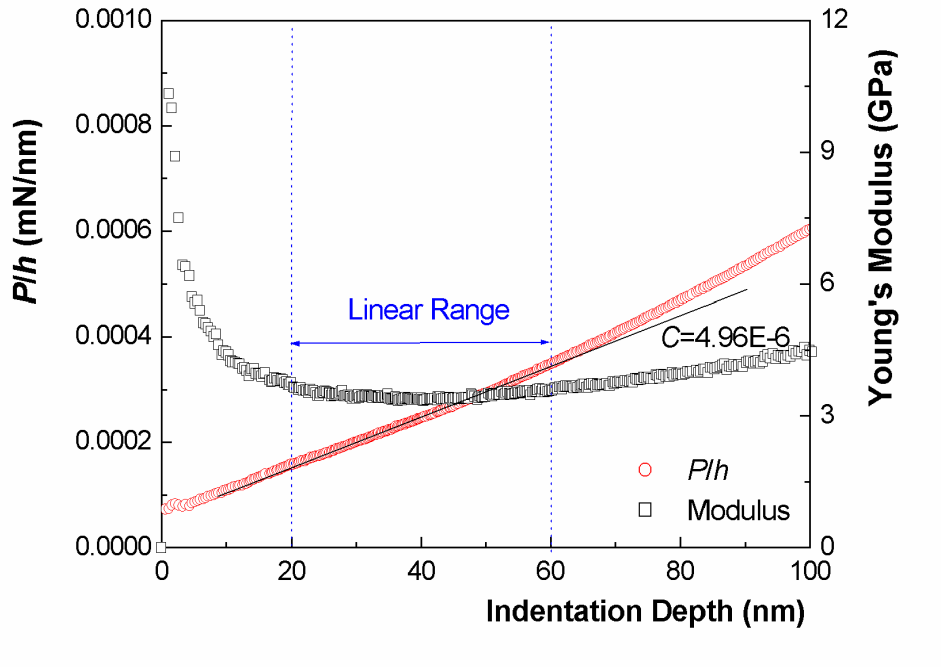

Fig. 3.5 Young's modulus versus indentation depth curve and *P*/*h* versus indentation depth curve for XLK^{TM} (k=2.0) porous low-k thin film in the range of nano-indentation depth is less than 100 nm.

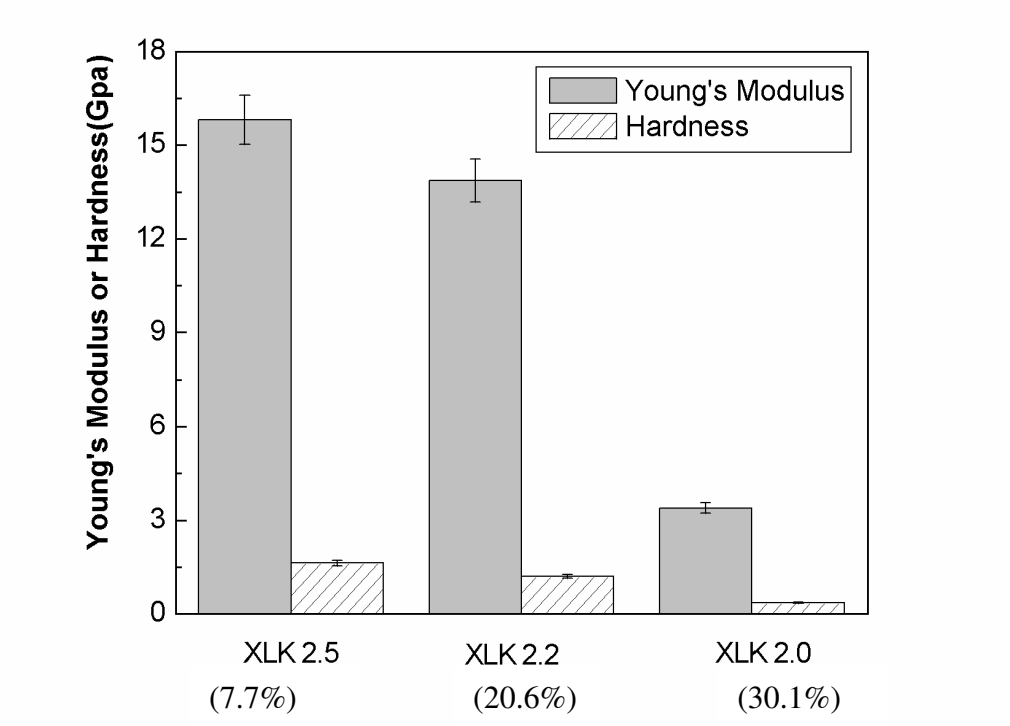

Fig. 3.6 Young's modulus and hardness versus porosity.

The results of Young's modulus and hardness of the three XLK^{TM} porous low-*k* thin films are shown in Fig. 3.6. The average value and the standard deviation of each film are obtained by ten indentation tests. The standard deviation of each case is found to be small. The differences of Young's modulus and hardness among the three films are statistically significant. Both Young's modulus and hardness decrease with the porosity. The decrease of Young's modulus and hardness is particularly large when the porosity of the XLK^{TM} film is increased from 20.6% to 30.1%. The sharp drop in mechanical properties of XLK^{TM} porous low-*k* thin films may be explained by the following empirical relation [4, 5]

$$\frac{E}{E_0} = (1 - \frac{P}{P_c})^f \tag{3-2}$$

$$\frac{H}{H_0} = (1 - \frac{P}{P_c})^f \tag{3-3}$$

where E and H are the Young's modulus and hardness of the material under study, respectively; E_0 and H_0 are Young's modulus and hardness of the ideal fully dense material, respectively; f is the percolation exponent which is an empirical constant; P is the porosity of the material, P_c is the percolation threshold at which Young's modulus reduces to zero.

Fitting our data into the empirical relation determines the values of P_c and f to be 30.11% and 0.18, respectively. A comparison of the data and the fitting result is depicted in Fig. 3.7. Therefore, the porosity of the film has to be less than 30% in order to maintain the mechanical strength of the film. This finding is consistent with the

literature result. When more pores are introduced to reduce the dielectric constant, a percolation point will be reached where the pores become interconnected. The percolated pore structure may induce a sharp drop in the strength and other material properties of low-*k* dielectrics [6]. The pore structure of this material was found to remain closed cell at porosity less than 25% [7]. Therefore, the mechanical properties of XLK^{TM} porous low-*k* thin films drop abruptly when porosity changes from 20.6% to 30.1%.

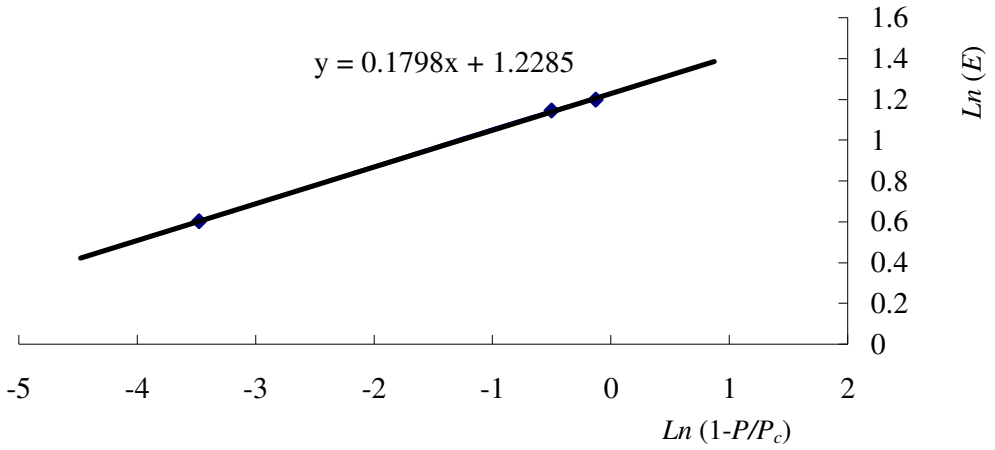

Fig. 3.7 Fitting curve for XLK^{TM} thin films (P_c=30.11%).

From the above results and discussion, it is evident that Young's modulus and hardness of the porous low-*k* film can be determined by the nano-indentation method. The nano-indentation results of the mechanical properties of the porous films shows that Young's modulus *E* and hardness *H* decrease as the porosity of the film is increased. The reduction of *E* and *H* is significant, more than 70%, when the porosity is higher than 30%. The result provides a guideline on the values of the porosity that can be adopted in the low-*k* films. The finding led us to focusing on the cases with the values of *k* larger

than 2.2 when we studied the effects of nitrogen plasma treatment on the mechanical strength of the porous films. This is presented in the next chapter.

References

[1] J. G. Ryan, Proc. of the low-*k* Dielectric Mater. Tech. Conf., 185 (SMICON WEST, 2000).

[2] R. Goldblatt, Proc. of IEEE Int. Interconnect Tech. Conf., 263 (2000).

[3] M. Morgen, E. T. Ryan, J. H. Zhao, C. Hu, T. H. Cho and P. S. Ho, Annu. Rev. Mater. Sci. 30, 645 (2000).

[4] E. O. Shaffer II, K. E. Howard, M. E. Mills, and P. H. Townshend, Mat. Res. Soc. Symp. Proc. 612, 1 (2000).

[5] X. Xiao, R. Streiter , H. Wolf, G. Ruan, C. Murray, and T. Gessner, Microelectron. Eng. 55, 53 (2001).

[6] J. J. Liu, D. W. Gan, C. Hu, M. Kiene, and P. S. Ho, Appl. Phys. Lett. 81, 4180 (2002).

[7] R. D. Miller, R. Beyers, K. R. Carter, R. F. Cook, M. Harbison, C. H. Haerker, J. L. Hederic, V. Lee, E. Liniger, C. Nguyen, J. Remenar, M. Sherwood, M. Trollsas, W. Volksen, and D. Y. Yoon, Mater. Res. Soc. Symp. Proc. 565, 3 (1999).

Chapter 4. Effects of NH_3 Plasma Treatment on Mechanical Properties of Porous Low-*k* Thin Films

In Chap. 3, the effects of film porosity on Young's modulus and hardness of low-*k* thin films measured by the nano-indentation method have been presented and discussed. It showed that the pores in the low-*k* thin films degrade the mechanical properties of the thin films. The weak mechanical properties may cause many challenges in manufacturing process, such as cracking and delamination during packaging process. In order to improve the mechanical properties of porous low-*k* thin films, plasma treatment was implemented on porous low-*k* thin films. Section 4.1 demonstrates that Young's modulus and hardness of ZIRKON LK2200^{TM} porous low-*k* thin film can be improved by NH_3 plasma treatment, followed by an investigation of the mechanism that results in the improvement of the mechanical strength of the porous low-*k* thin film. Section 4.2 addresses the effectiveness of the NH_3 plasma treatment on the mechanical properties of another porous low-*k* thin film, LKD5109^{TM} porous low-*k* thin film supplied by JSR.

4.1 Effects of NH_3 Plasma Treatment on the Mechanical Properties of ZIRKON LK2200^{TM} Porous Low-*k* Thin Films

The focus of this section is on the effects of NH_3 plasma treatment on the mechanical properties of ZIRKON LK2200^{TM} porous low-*k* thin film, a MSQ-based thin film. The *k* value of the ZIRKON LK2200^{TM} porous low-*k* thin film is 2.2 and the

thickness of the thin film is about 1 酸 The pores in the film are tubular shaped as revealed by positronium annihilation lifetime spectroscopy (PALS) measurement. The average size of the pores is 2.7 nm and the percolation length is 300 nm. Details of the ZIRKON LK2200^{TM} porous low-*k* thin films are briefly discussed earlier in Sec. 2.3. The ZIRKON LK2200^{TM} porous low-*k* thin films were treated in the ORION^{TM} plasma enhanced chemical vapor deposition (PECVD) system. The NH_3 plasma treatment used in this project is described in Sec. 2.3.

The effects of NH_3 plasma treatment on the ZIRKON LK2200^{TM} porous low-*k* thin film is characterized by nano-indentation method in combination with SIMS, TEM, and FTIR. The results show that the plasma treatment leads to significant improvement of the mechanical properties of the film due to the formation of a non-porous dense skin layer.

4.1.1 Young's Modulus and Hardness of ZIRKON LK2200^{TM} Porous Low-*k* Thin Films after Plasma Treatment

Fig. 4.1(a) shows Young's modulus of the ZIRKON LK2200^{TM} porous low-*k* thin films before and after plasma treatment. The plasma treatment time is 10, 30, and 60 seconds, respectively. Young's modulus measured by the nano-indentation method varies with the indentation depth. Fig. 4.1(a) shows the overall trend of Young's modulus versus indentation depth. It can be seen that, near the surface, Young's modulus values decrease with increasing indentation depth before they reach certain minimum values. This decrease of the measured value with indentation depth near the free surface

is typically due to the surface effect and other factors. After reaching the minimum values, there is a short range in which the measured Young's modulus remains constant. Beyond the constant range, the measured values of Young's modulus increase gradually with the further increasing indentation depth because of the substrate effect. Finally, Young's moduli of the films with the different treatment time come to almost the same value.

The improvement of Young's modulus of the plasma treated films in the near surface range (around 100 nm) is shown clearly in Fig. 4.1(b). In this range, the measured Young's moduli of the plasma treated films with longer plasma treatment time have higher value at the same indentation depth. The higher Young's modulus of the treated films at small indentation depth can be caused by two mechanisms: the surface roughness and the plasma treatment. To investigate whether the enhancement comes from the surface roughness or not, we measured the RMS surface roughness of the as-received and treated films by AFM and the results are listed in Table 4.1. The results suggest that the surface roughness of all of the films before and after plasma treatment is of the order of the magnitude of 10 nm. Since the values of the surface roughness are similar for all measured films, the effect of the surface roughness on Young's modulus would not change significantly. This leads to the conclusion that the enhancement of Young's modulus at small nano-indentation depth is not caused by the surface roughness effect. Instead, the enhancement is a consequence of the NH_3 plasma treatment. The actual mechanism of the enhancement is examined later in the following Sec. 4.1.3.

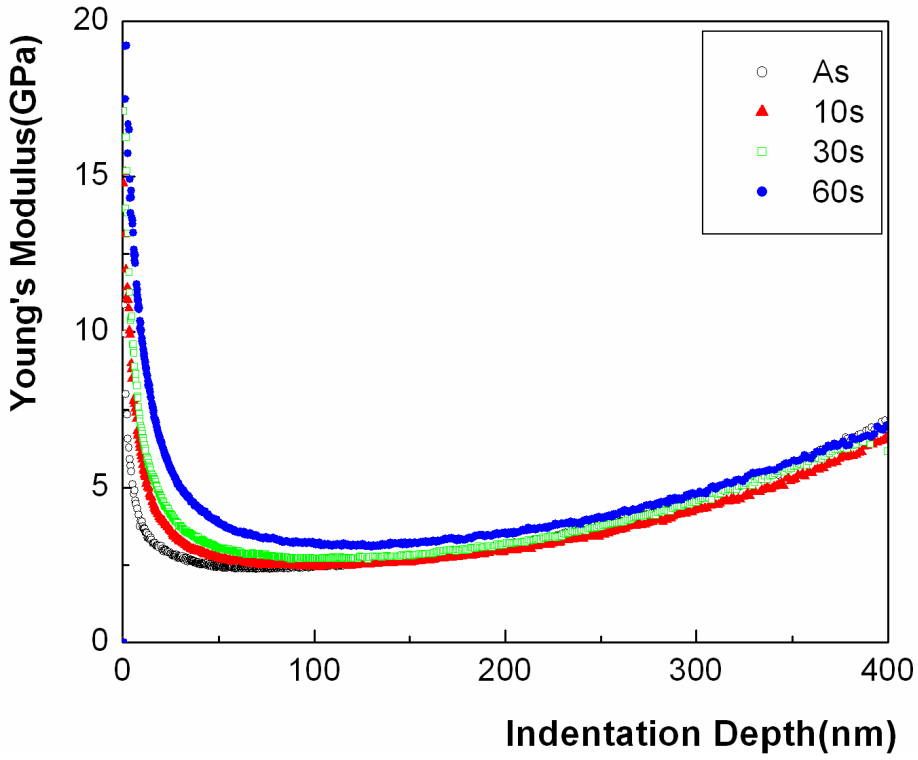

(a)

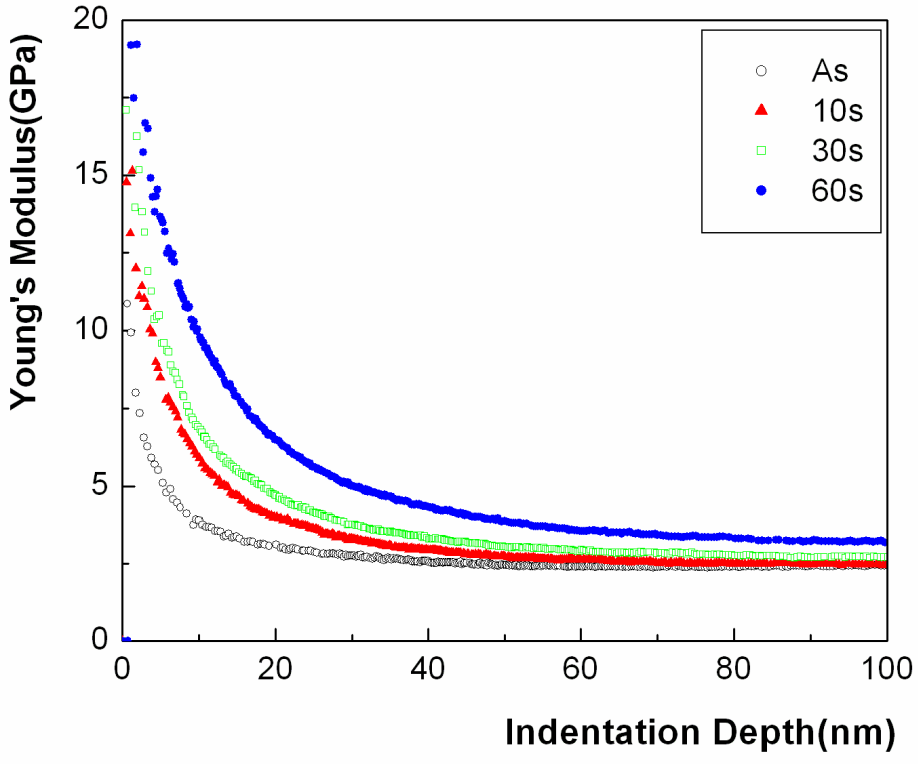

(b)

Fig. 4.1 (a) Young's modulus versus indentation depth curves for ZIRKON LK2200^{TM} porous low-*k* thin films after different plasma treat time: as-received, 10 s, 30 s, and 60 s. **(b)** Zoom-in plot at less than 100 nm indentation depth of (a).

Table 4.1 Surface roughness of ZIRKON LK2200^{TM} porous low-*k* thin films with different plasma treatment time.

Treat Time (s)	Surface Roughness (nm)
0	6 ± 0.3
10	11 ± 0.4
30	10 ± 0.4
60	12 ± 0.6

Fig. 4.2 shows the hardness of the ZIRKON LK2200^{TM} porous low-*k* thin films before and after NH_3 plasma treatment. The NH_3 plasma treatment time was 10, 30, and 60 seconds, respectively. Fig. 4.2(a) plots the results with the indentation depth less than 400 nm, while Fig. 4.2(b) focuses on the range that the indentation depth is less than 100 nm. Similar to the results of Young's modulus in Fig. 4.1(a), the hardness varies with the indentation depth. The measured value of hardness decreases with the indentation depth at the beginning. After the value reaches the minimum, there is a constant range in which the hardness *H* is a constant. After this range, *H* increases slightly with the indentation depth due to the substrate effect. The results in Fig. 4.2(b) also indicate at small indentation depth, the longer the plasma treatment time is, the higher the hardness is at the same indentation depth. In addition, the differences in hardness between the plasma-treated and the as-received films decrease with the indentation depth. Finally, the measured hardness becomes almost the same when the indentation depth exceeds 300 nm for all films. Similar to the enhancement of Young's modulus, the enhancement of hardness also results from the NH_3 plasma treatment.

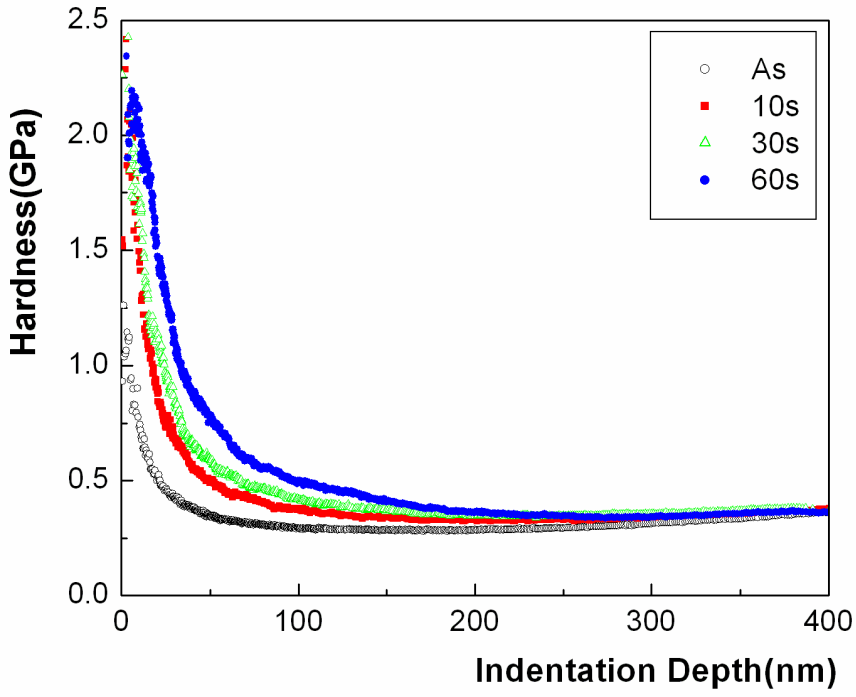

(a)

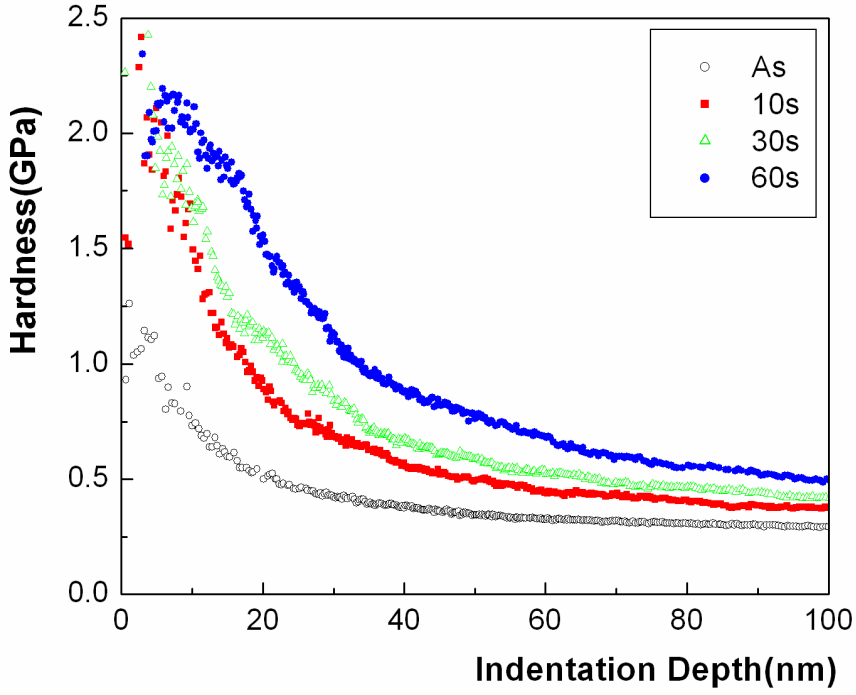

(b)

Fig. 4.2 (a) The hardness versus indentation depth curves for ZIRKON LK2200^{TM} porous thin films after different plasma treatment time: as-received, 10 s, 30 s, and 60 s. **(b)** Zoom-in plot at less than 100 nm indentation depth of (a).

From above results we can conclude that the NH_3 plasma treatment enhanced significantly Young's modulus and hardness at the near surface region of the ZIRKON LK2200^{TM} porous low-*k* thin films. To further understand the enhancement of Young's modulus and hardness at small indentation depth, the method developed in Chap. 3 for determining the mechanical properties of thin films is used in the following section.

4.1.2 Analysis of *P/h* versus Indentation Depth

Fig. 4.3(a) shows the *P/h* versus indentation depth curves for the ZIRKON LK2200^{TM} porous low-*k* thin films with different plasma treatment time. The slop of the curve, called the indentation resistance *C*, reveals the mechanical properties of the film. For the untreated porous film, the slop *C* is a constant, denoted as C_0, in the range of indentation depth adopted in our experiment. For the films treated with NH_3 plasma, the slop *C* at small indentation depth *h* is higher than the value C_0 of the untreated film, while the slop approaches C_0 as the indentation depth increases. It is also found in the figure that the initial slope *C* increases with the plasma treatment time. The higher value of *C* at small *h* suggests a harder layer forms at the surface of the porous film during the treatment. A schematic diagram of the possible structure of the porous film is depicted in Fig. 4.3(b). The layer developing on the top of the film may be phase with the composition, the porosity, and the density being different from those of the original porous low-*k* thin film. The hard top layer might have resulted from the ion bombardment during the plasma process and the chemical reaction between the NH_3 plasma and the film. It is the top layer that leads to the enhancement of Young's modulus,

hardness, and *C* at small indentation depth. The composition and structure of the top layer are further discussed in Sec. 4.1.3.

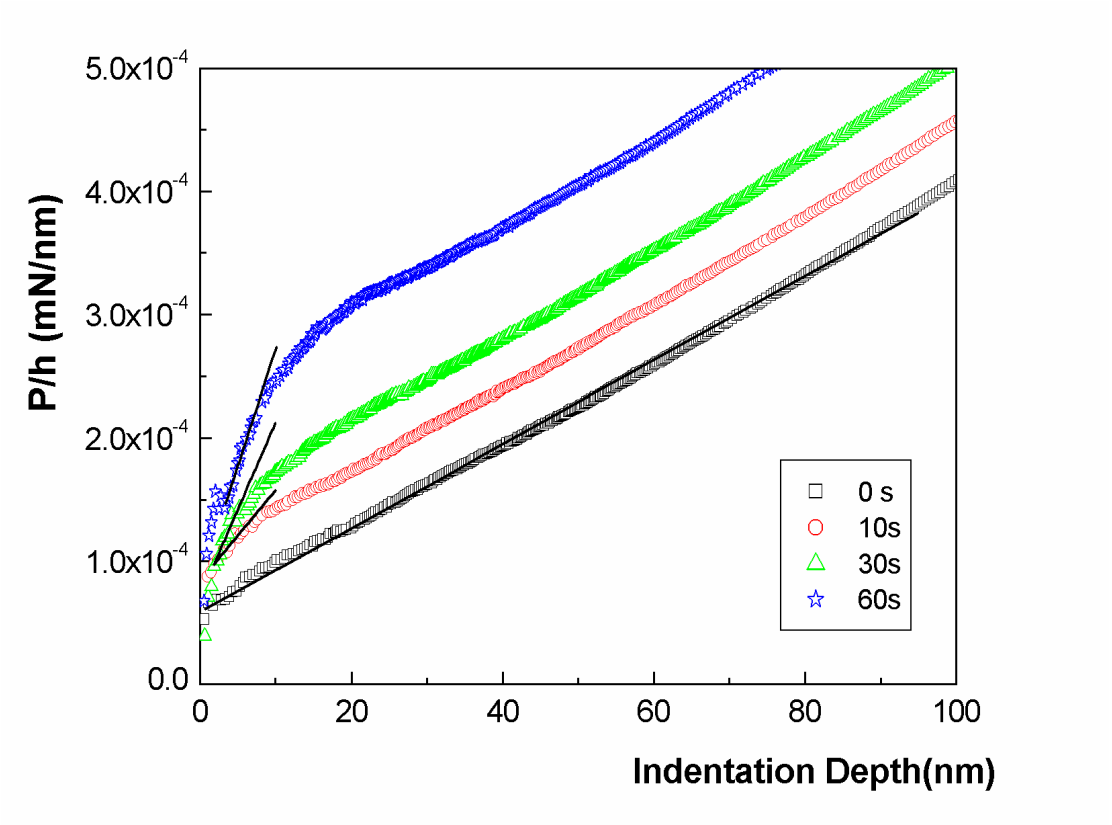

(a)

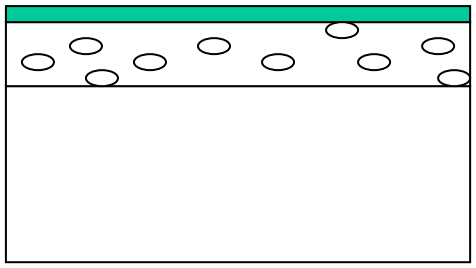

Dense Layer

MSQ Porous Low-*k* thin film

Si Substrate

(b)

Fig. 4.3 (a) *P*/*h* versus Indentation Depth curves for ZIRKON LK2200^{TM} porous thin films after different plasma treat time: as-received, 10 s, 30 s, and 60 s. **(b)** Structure of ZIRKON LK2200^{TM} porous thin films after plasma treatment.

From the change of the *C* value in Fig. 4.3, we can estimate the thickness of the dense layer formed and the results are listed in Table 4.2. It is important to note that, though the calculated thickness of the top layer increases with the increasing plasma treatment time, the dense layer remains very thin compared with the thickness of the porous low-*k* thin film even for 60 s of plasma treatment. Table 4.2 also summarizes the indentation resistance *C* of as-received and plasma treated thin films at small indentation depth. The indentation resistance in the table is determined by taking the average of *C* of ten repeated tests. The *C* value is 3.41 for as-received porous low-*k* thin film. After plasma treatment, it increases to 7.4, 14.1 and 18.8 for 10 s, 30 s, and 60 s plasma treatment, respectively.

Although it is evident in our experimental results that the measured Young's modulus is increased in the top layer after NH_3 plasma treatment, it is difficult to determine the actual value of Young's modulus of dense top layer. The issue of determining Young's modulus of the top layer of the porous film after the NH_3 treatment was resolved by the following method.

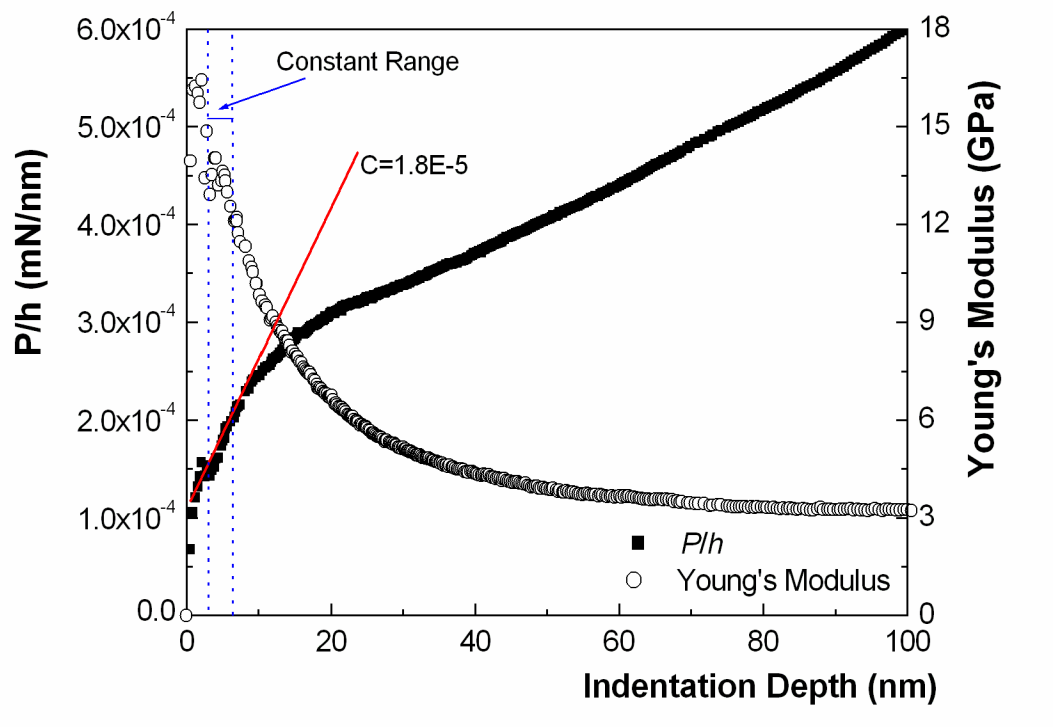

(a)

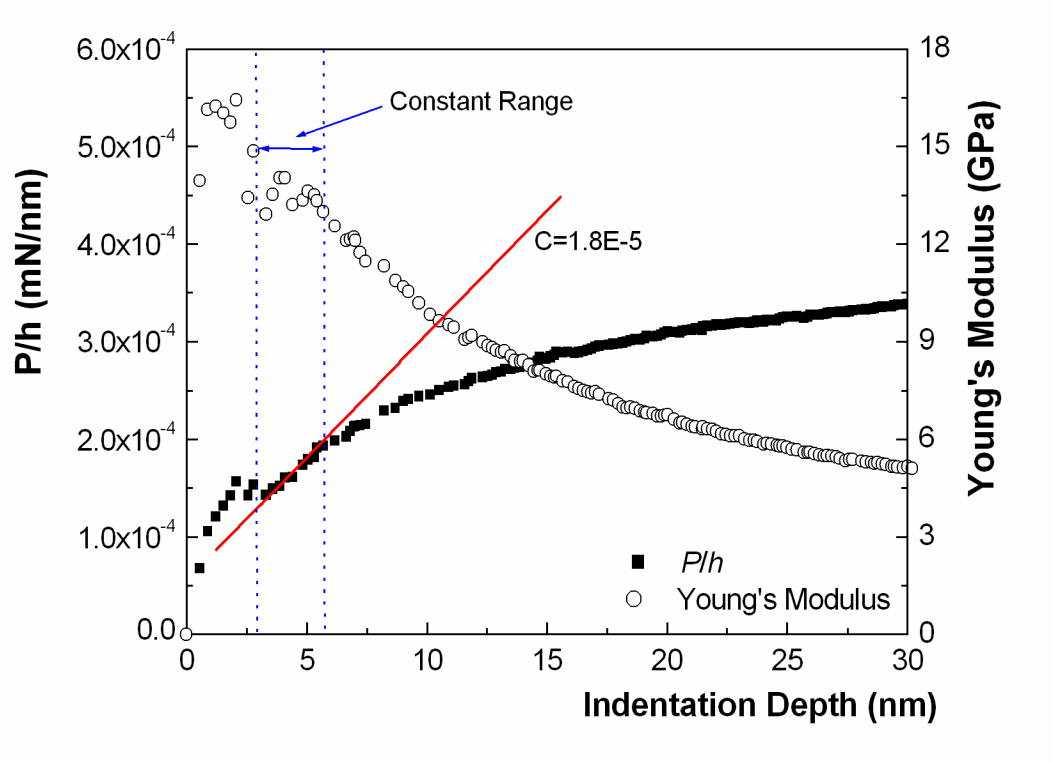

(b)

Fig. 4.4 (a) *P*/*h* versus indentation depth curve and Young's modulus versus indentation depth curve for the porous ZIRKON LK2200^{TM} thin films after 60 s NH_3 plasma treatment. **(b)** Zoom-in plot at less than 30 nm indentation depth of (a).

Fig. 4.4 shows Young's modulus versus indentation depth curve and *P/h* versus indentation depth curve for the sample with 60 seconds exposure time in NH_3 plasma. The figure indicates a range of indentation depth in which Young's modulus remains constant and the *P/h* versus indentation depth curve is linear. This special range, as discussed in Chap. 3, can be adopted to determine Young's modulus and hardness of the top layer without significant influences of the surface roughness and the different mechanical properties of the materials below the top layer. In our study, Young's modulus and hardness of the top surface layer are determined by taking the average of the values in the range. To increase the accuracy of the results, the nano-indentation experiment was carried out 10 times to collect the mechanical properties of the top surface layer. The results of the average and the standard deviation derived from the experiments are summarized in Table 4.2.

Table 4.2 *C*, thickness, Young's modulus, and hardness for dense layer of ZIRKON LK2200^{TM} porous thin films after different plasma treatment time

Treated Time (S)	C X10^6 (mN/nm^2)	Thickness of Dense Layer (nm)	Young's Modulus of Dense Layer (GPa)	Hardness of Dense Layer (GPa)
0	3.41 ± 0.15	0	2.42 ± 0.12	0.30 ± 0.02
10	7.40 ± 0.39	9.4 ± 1.5	6.84 ± 0.43	1.61 ± 0.07
30	14.1 ± 0.73	12.8 ± 2.4	10.03 ± 0.51	1.79 ± 0.09
60	18.8 ± 0.91	21.2 ± 3.8	13.69 ± 0.69	1.86 ± 0.12

It shows clearly that the longer plasma treatment leads to higher Young's modulus and hardness in Table 4.2. Young's modulus is improved from 2.42 GPa to 13.69 GPa and the hardness is improved from 0.30 GPa to 1.86 GPa after 60 seconds plasma

treatment. The results satisfy the hardness requirement for packaging [1]. Although the hardness increases with the plasma treatment time, the improvement is the most significant in the first 10 seconds, after 10 seconds of plasma treatment, the hardness changes slightly with the plasma treatment time. This finding suggests the structure and the composition of the top layer do not change significantly after its formation. The thickness of the dense layer is very thin, thus the main structure of the ZIRKON LK2200^{TM} porous thin films did not change.

4.1.3 Mechanism of the Formation of the Hard Layer by NH_3 Plasma Treatment

In order to further verify the formation of the thin dense layer at the surface of porous low-*k* thin films, TEM was adopted to analyze the microstructure of ZIRKON LK2200^{TM} porous low-*k* thin films after NH_3 plasma treatment. The TEM result of LK2200^{TM} porous thin film after 10 seconds plasma treatment is shown in Fig. 4.5. The figures in both low and high magnifications indicate there is a thin dense layer on top of the film. The picture shows that the thickness of the dense layer is about 10 nm when the treatment time is 10 seconds. The thickness is in good agreement with that estimated from the nano-indentation tests. The TEM results also confirm that the NH_3 plasma treatment does not cause damage on the surface; instead, the treatment generates a layer of different structure.

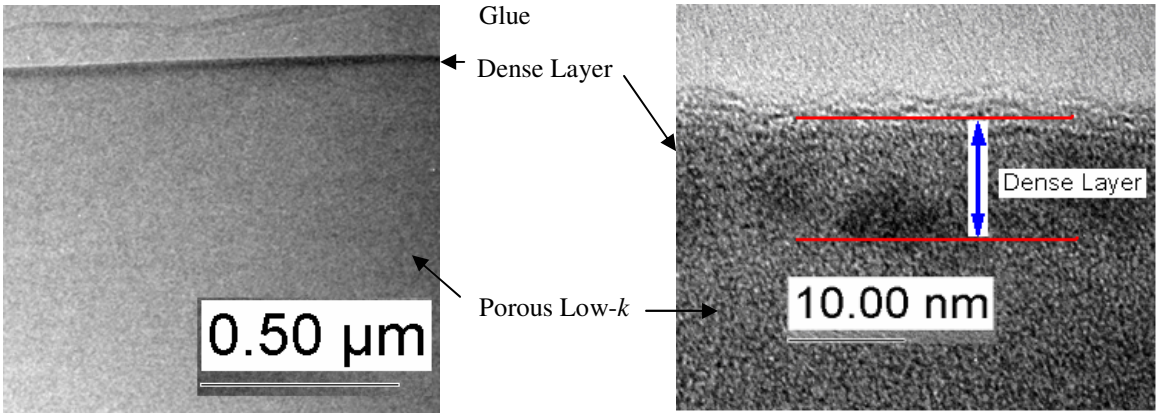

Fig. 4.5 Cross-section of ZIRKON LK2200^{TM} porous thin film after 10 s NH_3 plasma treatment. **(a)** at low magnification; **(b)** at high magnification.

In order to further illuminate the mechanism that causes the enhancement of mechanical properties, SIMS analysis was carried out to evaluate the variation of element concentration with the thin film depth. The result of the carbon concentration is shown in Fig. 4.6(a). The results indicate the carbon atoms are depleted during the plasma treatment and the width of the carbon depletion region increases with the treatment time. The result of the nitrogen concentration is illustrated in Fig. 4.5(b). The results in Fig. 4.6(b) show the incorporation of N atoms in the porous film. The positions of the peaks of the curves reveal the depth of the N incorporation, and it is found that the depth increases with the plasma treatment time. The depth is about 180 nm for the film subject to 60 seconds of treatment.

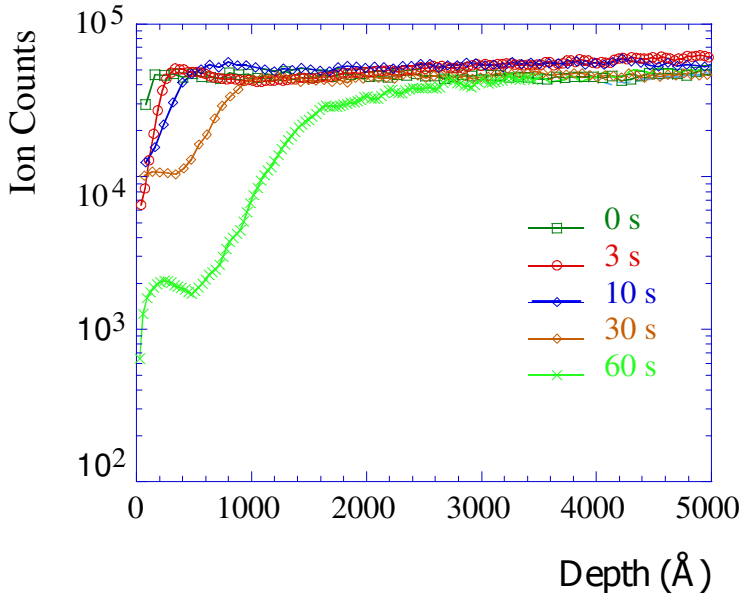

(a)

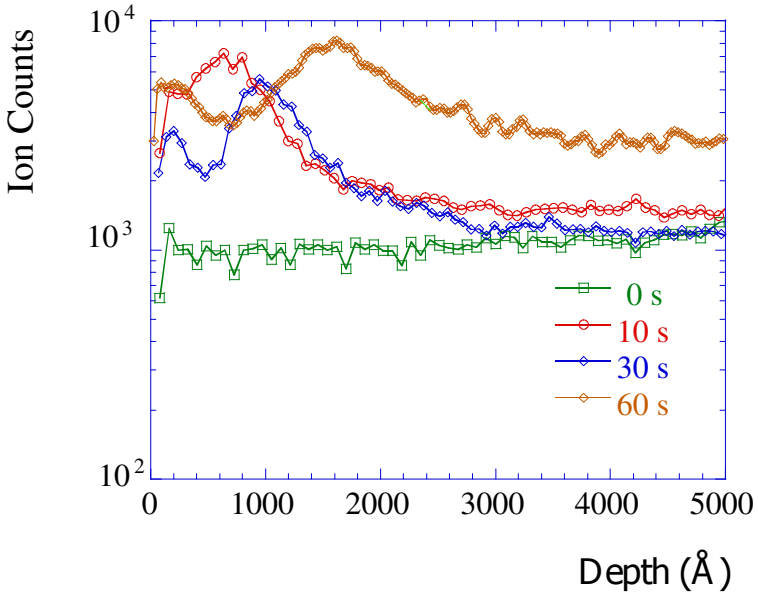

(b)

Fig. 4.6 (a) SIMS carbon profiles of ZIRKON LK2200^{TM} porous thin films after different plasmas treatment time. **(b)** SIMS nitrogen profiles of ZIRKON LK2200^{TM} porous thin films after different plasmas treatment time.

The depletion of carbon and the incorporation of nitrogen suggest that some kind of chemical reactions occur during the plasma treatment process near the surface region. A possible scenario of the chemical reaction can be described as follows. First, after plasma generation, nitrogen-containing radicals and ions, such as H^+, quickly diffuse into open nano-pores in the surface region. The ion H^+ can react with the carbon in the film to form the volatile CH_4, while the nitrogen-containing radicals react with SiO_2 to form $SiON_X$, a compound with stronger mechanical properties. The close of the pores may also be assisted by the bombardment of the ions during the plasma process. The formation of SiONx and the close of pores yield the dense surface layer that contributes to the improvement of the mechanical properties of the structure as observed in the nano-indentation experiments. The formation of a thin $SiON_X$ by the nitrogen based plasma treatment was also reported previously on non-porous MSQ thin film [2].

The width of the plasma modified surface regions estimated by the SIMS analysis is found to be between 20 to 200 nm, which is larger than the thicknesses of the dense surface layers observed in the nano-indentation and the TEM experiments. The finding suggests that the structure of the porous film after the plasma treatment can be divided into three parts. On the surface of the film is a dense chemically modified layer that plays a crucial role in the improvement of the mechanical properties of the film. Below the top thin dense layer is a thicker regime, about 180 nm, characterized by carbon depletion and nitrogen incorporation. The porosity of this regime, however, is probably high; as a consequence, the regime has little effects on the mechanical properties of the film as demonstrated in our nano-indentation experiments. Below the regime of a

different chemical composition is the original porous film. It is necessary to explain our finding that the thickness of the dense layer does not increase significantly after 10 seconds plasma treatment. The dense layer can form quickly at the initial stage because the porous film is exposed to the plasma directly; thus, there is abundant supply of ions and radicals to fill the pores. After the dense layer is formed, the ions and radicals need to diffuse through the dense layer in order to reach the porous film. As a consequence, there is a limited supply of ions and radicals, making it difficult to fill the pores to form a dense layer.

FTIR was carried out to investigate the chemical compositions and structures in the bulk region of the ZIRKON LK2200^{TM} porous low-*k* thin films before and after the NH_3 plasma treatment. The results of different plasma treatment time are shown in Fig. 4.7. The results indicate that the relative intensity of the peaks corresponding to the cage (1150 cm^{-1}) and the network (1070 cm^{-1}) Si-O did not change significantly after the plasma treatment. No noticeable changes are observed either for other peaks. These results demonstrate that the chemical compositions and the structures of the bulk ZIRKON LK2200^{TM} porous low-*k* thin film remain unchanged after plasma treatment. It is in accordance with the conclusion deduced from nano-indentation, SIMS and TEM that the top surface layer that is improved to yield the better mechanical properties of the system.

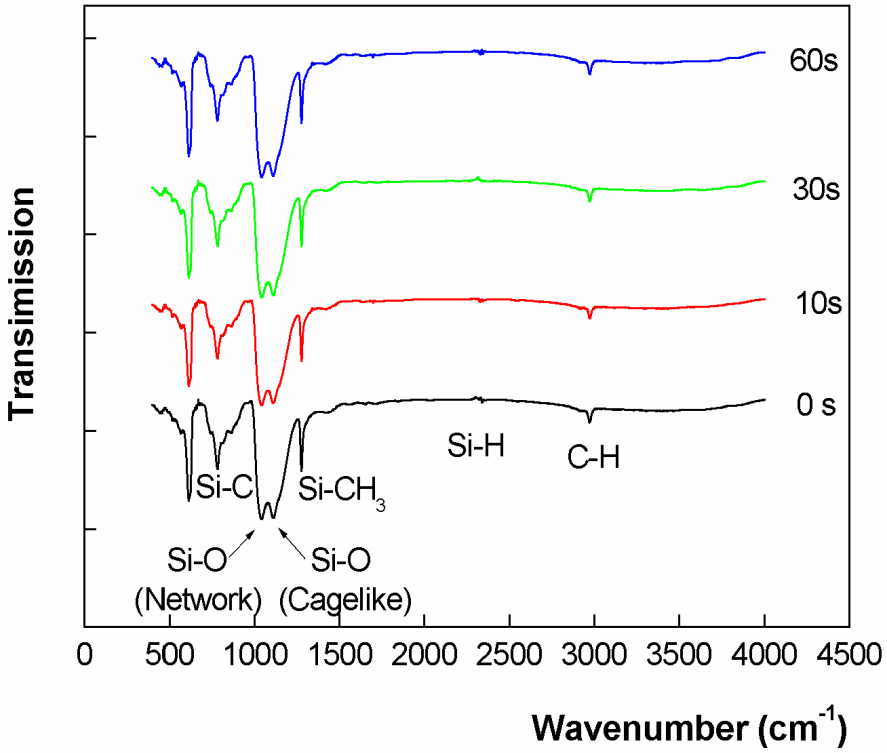

Fig. 4.7 FTIR spectra of ZIRKON LK2200^{TM} porous thin films after different plasma treatment time.

From above evidences, it is very obvious that the near surface region has been modified by the plasma treatment, while the structure and the chemical composition of the bulk porous low-*k* thin film layer remain intact. The significant improvement of the mechanical strength of the ZIRKON LK2200^{TM} porous low-*k* thin films due to the NH_3 plasma treatment suggests that the treatment may also be applied to other MSQ porous low-*k* thin films. The application of the technique to other types of porous films is demonstrated in the next section by considering the LKD5109^{TM} film.

4.2 Improvement of Mechanical Properties of Other Porous Low-*k* Thin Films after NH_3 Plasma Treatment

The results in the previous section suggest that the plasma treatment can improve the mechanical properties of porous low-*k* thin film mainly due to the formation of non-porous skin layer on the film surface. Since the formation of the non-porous dense layer may be affected by the microstructures of the surface nano-pores such as pore length (or interconnectivity) in the film prior to the plasma treatment, the effectiveness of the plasma treatment may depend on the pore length of the thin porous film. The dependence of the plasma treatment on the pore length is investigated in this section by studying the plasma treatment effect on the mechanical properties of a porous film with long pore length. The film studied in this section is LKD5109^{TM} porous low-*k* thin film, a MSQ based porous thin film supplied by JSR. The LKD5109^{TM} film has the same chemical composition, porosity and dielectric constant as the ZIRKON LK2200^{TM} film. The average pore length of LKD5109^{TM} film is larger than 8000 Å as revealed by PALS measurement (done at the University of Michigan). In comparison, the average pore length of the ZIRKON LK2200^{TM} film examined in the previous section is about 3000 Å. Other information of the two porous thin films can be found in Sec. 2.5. The LKD5109^{TM} film was subject to the same NH_3 plasma treatment and the same nano-indentation method for characterizing the mechanical properties of the film.

Fig. 4.8 plots the variation of Young's modulus of the LKD5109^{TM} thin films with the nano-indentation depth after different NH_3 plasma treatment time. Fig. 4.8(a) shows the overall trend of the variation. Similar to the case of ZIRKON LK2200^{TM} thin film,

the measured Young's modulus *E* decreases with increasing indentation depth *h*, reaches a minimum value, and then increases with the indentation depth. The decrease in the measured values of *E* is typically due to the surface effect and other artifacts, while the increment of *E* at larger indentation depth is caused by the substrate effect. Comparing the results of different plasma treatment time clearly reveals that Young's modulus has been improved by the plasma treatment. The effect of the plasma treatment is particularly strong when the indentation depth is small, as shown in Fig. 4.8(b) which depicts the result in the range where the indentation depth is less than 50 nm. The indentation results of the JSR LKD5109^{TM} films are similar to that of the ZIRKON LK2200^{TM} films. The increment of Yong's modulus due to the plasma treatment in the current case is as high as that in the ZIRKON LK2200^{TM} film. The result demonstrates that the effectiveness of the plasma treatment is insensitive to the pore length of the film even when the length is as high as 8000 Å.

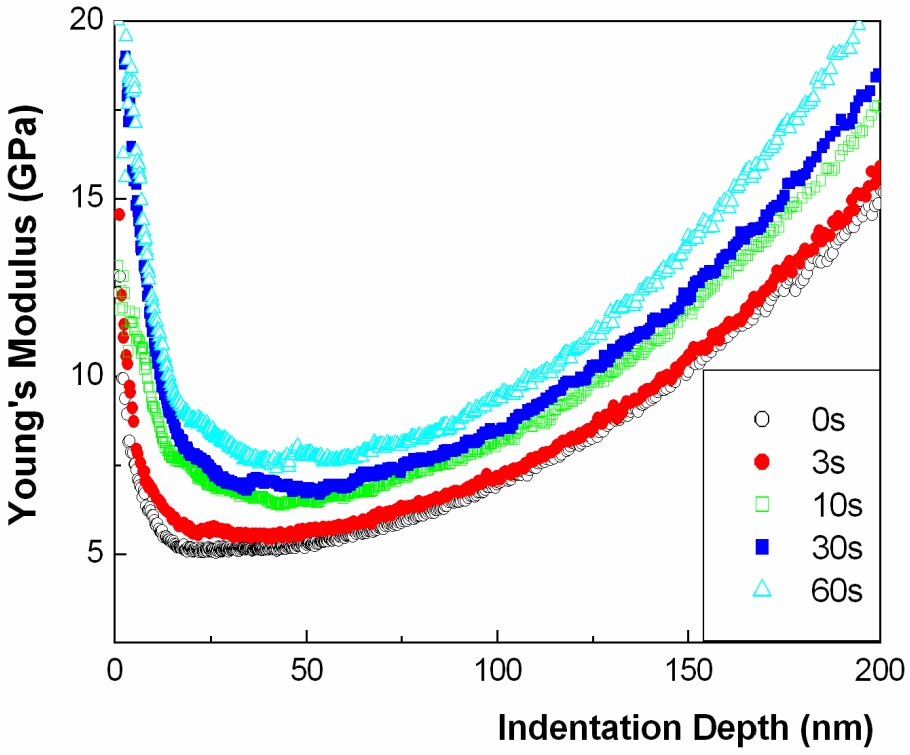

(a)

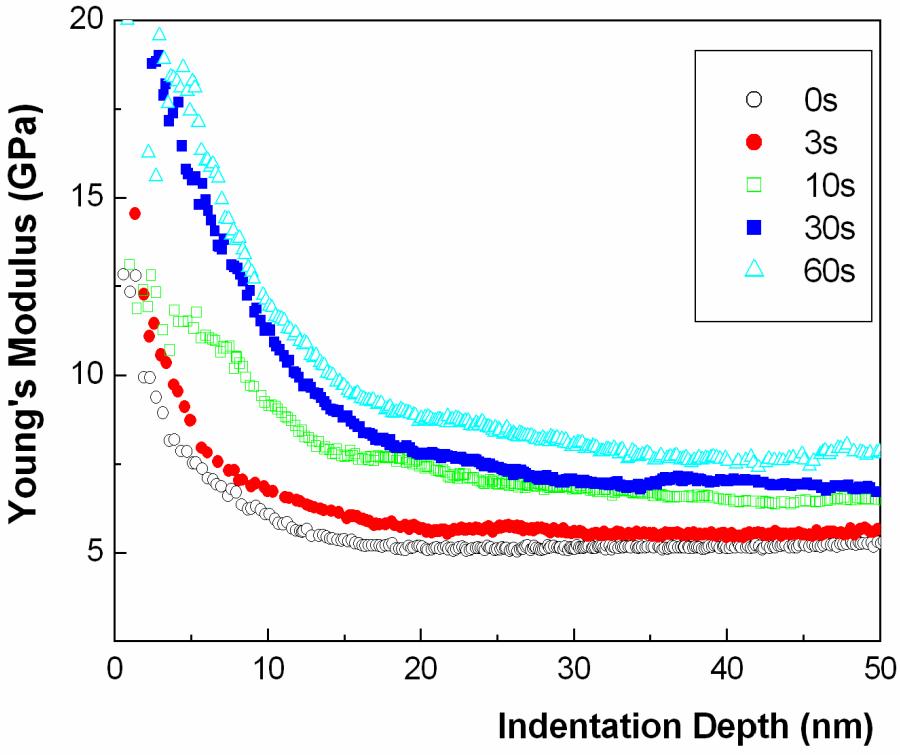

(b)

Fig. 4.8 Young's modulus of LKD5109™ porous low-*k* thin films with different plasma treatment time versus indentation depth.

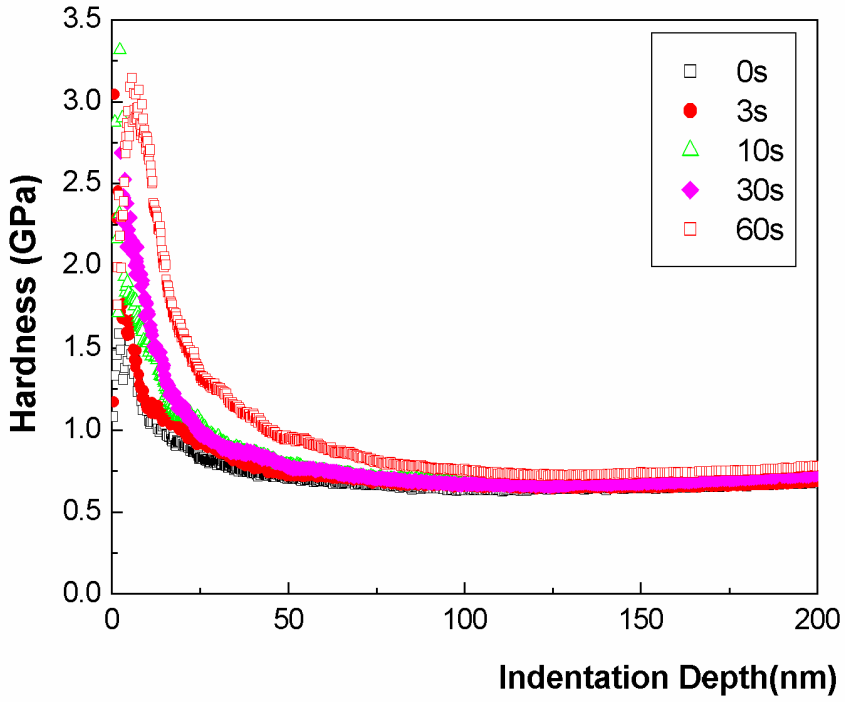

(a)

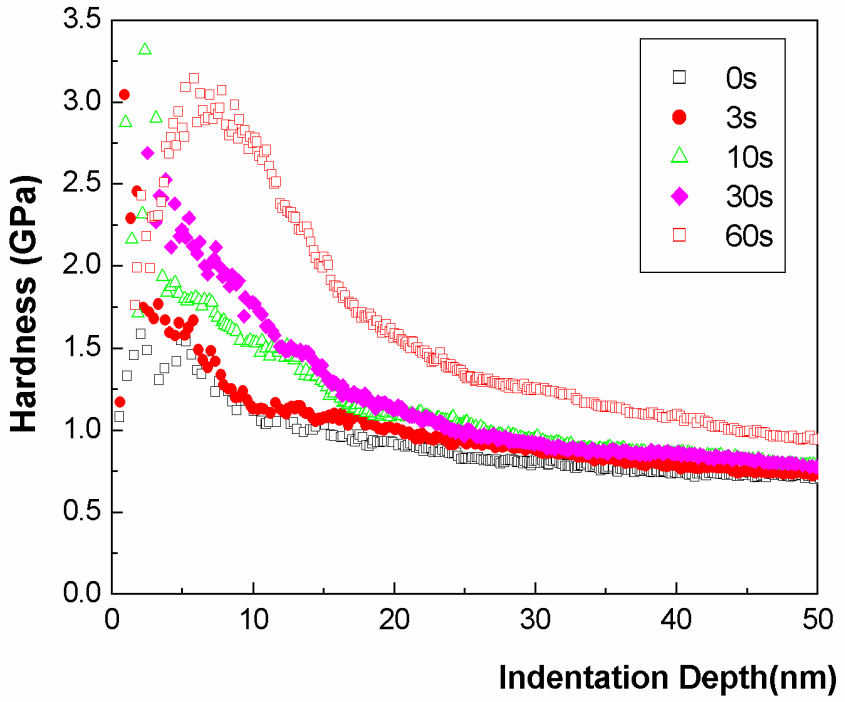

(b)

Fig. 4.9 Hardness of LKD5109^{TM} porous low-*k* thin films with different plasma treatment time versus indentation depth.

Fig. 4.9 shows variation of the hardness with the indentation depth for the LKD5109^{TM} thin films after subject to different plasma treatment time. The results indicate the hardness increases first, reaches a maximum, decreases, and approaches a constant as the indentation depth increases. At small indentation depth, the longer the plasma treatment time is, the higher the hardness is. Longer plasma treatment time also leads to higher maximum and a wider range of indentation depth around the maximum hardness. The range is from 5 to 10 nm for the LKD5109^{TM} film after 60 seconds plasma treatment. The improvement due to the plasma treatment, however, decreases as the indentation depth is larger. Finally, when the indentation depth is larger than 100 nm, the measured hardness is the same for all of the films.

Fig. 4.10 shows the *P/h* versus indentation depth curves for LKD5109^{TM} samples. At small indentation depth, the indentation resistances *C*, i.e. the slope of *P/h* versus indentation depth, increases with the increasing plasma treatment time. At large indentation depth, in contrast, all the plasma treated porous low-*k* thin films have the same *C* value as that of untreated thin film. This means that only the near surface structure has been changed after the NH_3 plasma treatment as far as the mechanical properties are concerned. The results of the LKD5109^{TM} samples are similar to that of the ZIRKON LK2200^{TM} samples discussed in the previous section, suggesting the improvement may also come from a dense surface layer. The average values of *C* of the dense layer over ten repeated tests are summarized in Table 4.3. Following the procedure discussed in Sec. 4.1, the thickness of the dense layer can be deduced from the *P/h* versus indentation depth curves, and list the results in Table 4.3.

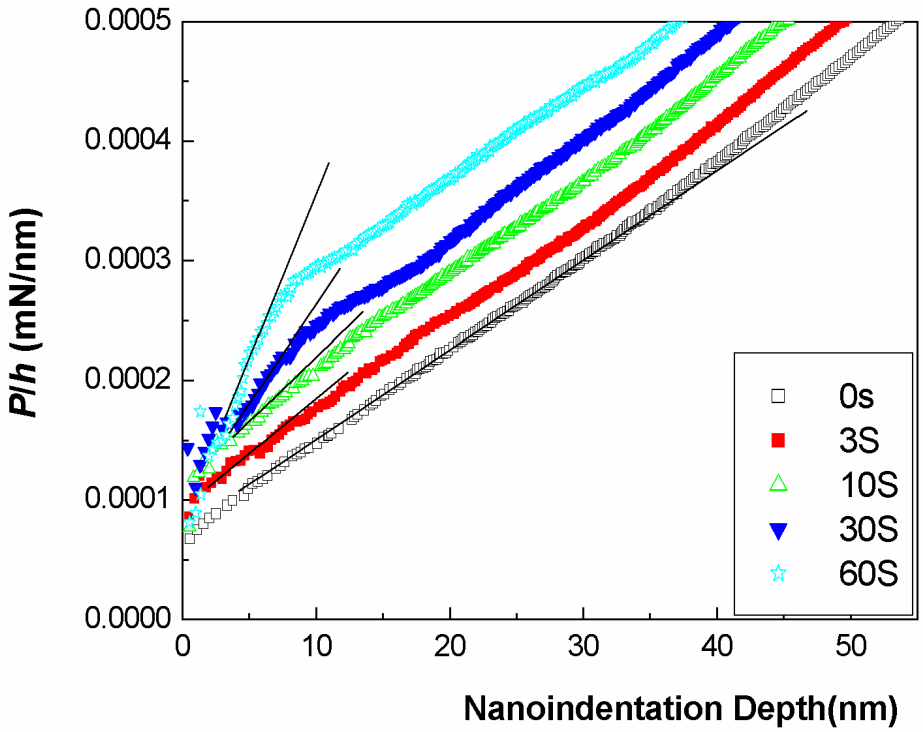

Fig. 4.10 *P/h* versus indentation depth curves for LKD5109^{TM} porous low-*k* thin films after different plasma treatment time (0 s, 3 s, 10 s, 30 s, 60 s).

Fig. 4.11 shows Young's modulus versus indentation depth curve and *P/h* versus indentation depth curve for the LKD5109^{TM} porous films with 60 seconds NH_3 plasma treatment. Combining the information of the two curves in Fig. 4.11 reveals that Young's modulus remains constant in the range where *P/h* versus indentation depth curve is linear. Using the same method described in the previous section, the value of the Young's modulus of the dense surface layer of the LKD5109^{TM} porous films can be obtained. Similarly, the hardness of the dense surface layer can also be determined by combining the hardness and *P/h* versus indentation depth curves. The average values of Young's modulus and hardness of the dense surface layer of the LKD5109^{TM} porous films are summarized in Table 4.3.

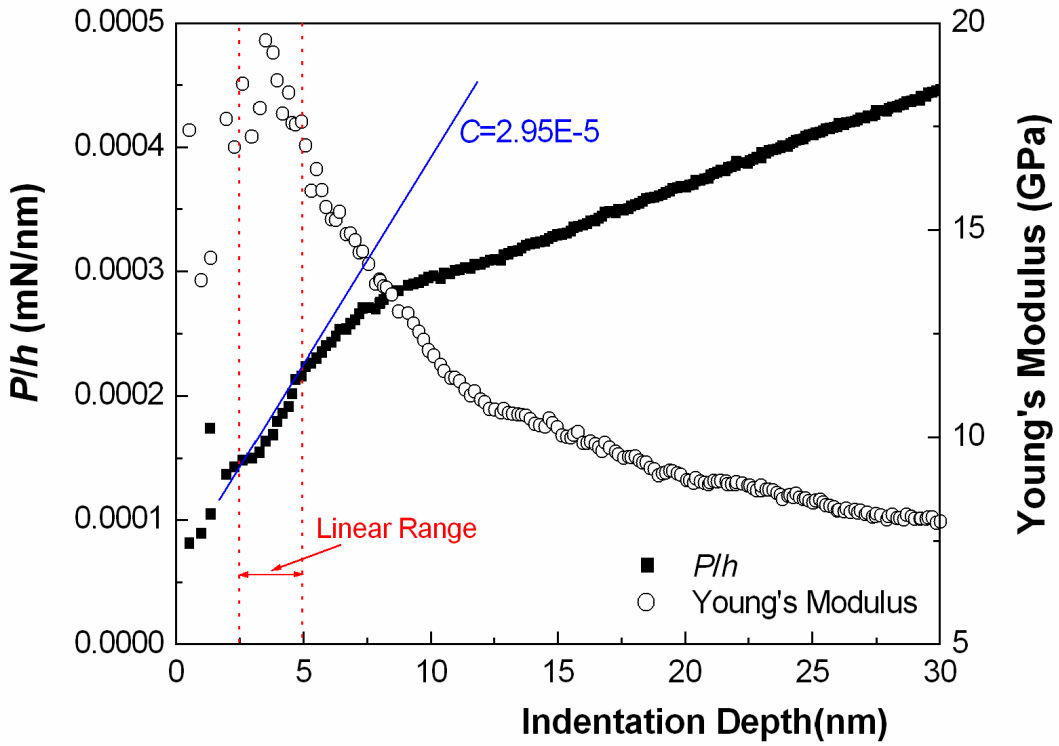

Fig. 4.11 *P*/*h* versus indentation depth curve and Young's modulus versus indentation depth curve for LKD5109^{TM} porous low-*k* thin film after 60 s NH_3 plasma treatment.

Table 4.3 *C*, thickness, Young's modulus, and hardness for dense surface layer of LKD5109^{TM} porous thin films after different plasma treatment time.

Treat Time (S)	*C* X10^6 (mN/nm^2)	Thickness (nm)	Young's Modulus (GPa)	Hardness (GPa)
0	7.6 ± 0.38	0	5.19 ± 0.26	0.64 ± 0.03
3	8.03 ± 0.41	8 ± 2	8.11 ± 0.40	1.36 ± 0.06
10	9.43 ± 0.47	10 ± 2	12.33 ± 0.61	1.69 ± 0.09
30	17.5 ± 0.87	10 ± 2	13.99 ± 0.69	1.90 ± 0.09
60	29.5 ± 2.1	10 ± 2	18.09 ± 0.91	2.42 ± 0.12

Table 4.3 shows that the plasma treatment enhances the mechanical properties of LKD5109^{TM} porous film by forming a surface dense layer. For example, Young' modulus of the dense layer is improved from 5.19 GPa to 18.09 GPa and the hardness of the dense layer is improved from 0.64 GPa to 2.42 GPa after 60 seconds plasma

treatment. Although the plasma treatment can generate a dense layer, the growth of the dense layer is not observed after the layer is formed. The main reason for this phenomenon has been explained later in the previous section. Besides the reason stated in the previous section, the longer pore length in the LKD5109^{TM} porous film makes the growth of dense layer more difficult after the formation of the dense surface layer because the longer pores are more difficult to be filled by ions and radicals. Therefore, the longer pore length does not affect the formation of the dense layer and the consequent improvement of mechanical properties even though the thickness of the dense layer is smaller and does not increase with the plasma treatment time after the formation of the dense surface layer.

The results in Secs. 4.1 and 4.2 suggest a general picture of the plasma treatment on MSQ-based porous low-*k* thin films. The plasma treatment typically leads to the formation of $SiON_X$ in the film and a skin dense layer on the top surface of the film. The dense skin layer plays a crucial role in the improvement of the mechanical properties of film. This improvement is insensitive to the pore length of the film if the initial porosity of the film is the same. This is due to the fact that the improvement of the mechanical properties is mainly determined by the porosity in the top dense surface layer, which is about the same as that in the non-porous films with the same chemical composition. The dense layer forms quickly within a short period of NH_3 plasma treatment, which is roughly 10 nm. Afterwards, the thickness of the dense layer increases slightly with the plasma treatment. Although the growth of the dense layer is slowed down significantly, the chemical composition of the remaining porous film can be changed by further

plasma treatment, leading to a thick porous layer of $SiON_X$. Therefore, it is desirable to perform the NH_3 plasma treatment on porous low-k films for short processing time to maximize the improvement of mechanical properties and to minimize adversary effects, such as the increase in effective dielectric constant due to the composition change.

4.3 Other Applications

In addition to the improvement of mechanical properties, another advantage of the plasma treatment on the porous low-*k* film is that the surface of the porous low-*k* film can be "sealed" to minimize diffusion of copper atoms into the dielectric film. The minimum thickness required for tantalum (Ta) to form a continuous barrier layer is affected by the pore size and the surface roughness of the porous low-*k* films [3]. The films with large pores require thick diffusion barrier layers to form effective diffusion barriers [4~6]. Therefore, the formation of thin dense layer on the surface of porous low-*k* thin film can reduce the requirement on the thickness of the diffusion barrier layer and thus reduce the effective dielectric constant of the whole stack, which includes the barrier layer and the porous low-*k* thin films. The effects of the plasma treatment on the sealing of the porous films have been confirmed by our collaborators for the ZIRKON LK2200 ^{TM} porous low-*k* thin film. Compared with the method of sealing the surface of porous low-*k* thin film with silica [7], the plasma treatment has more advantages. The plasma treatment can be easily introduced into the semiconductor manufacturing process by in-situ treatment after the reactive ion etch (RIE) process, while sealing surface with silica requires a two-layer deposition process which is complicated and

expensive. The sealing effect of the plasma treatment, however, is ineffective on the LKD5109^{TM} porous low-*k* thin film. This is attributed to the long pore length in this film. During the plasma treatment, the long pores make it difficult to develop a continuous dense surface layer that has the capability to prevent Cu diffusion though the mechanical properties of the top surface layer has been significantly improved.

The sealed dense layer of porous low-*k* thin film can also be employed to prevent the poisoning of photoresist. The chemical gas residue in the pores will cause poisoning of photoresist [8] as shown in Fig. 4.12(a). In order to solve the problem, hard masks were introduced. Fig. 4.12 (b) shows that the hard mask works in the case of single damascene structure. The hard-mask method, however, fails in the dual damascene structure because the chemical gas residue may diffuse through the sidewall and cause poisoning of photoresist as shown in Fig. 4.12(c). The problem can be resolved if the plasma treatment is applied after via etch. The dense layer formed at the surface of the porous low-*k* thin film can prevent poisoning of photoresist as shown in Fig. 4.12(d).

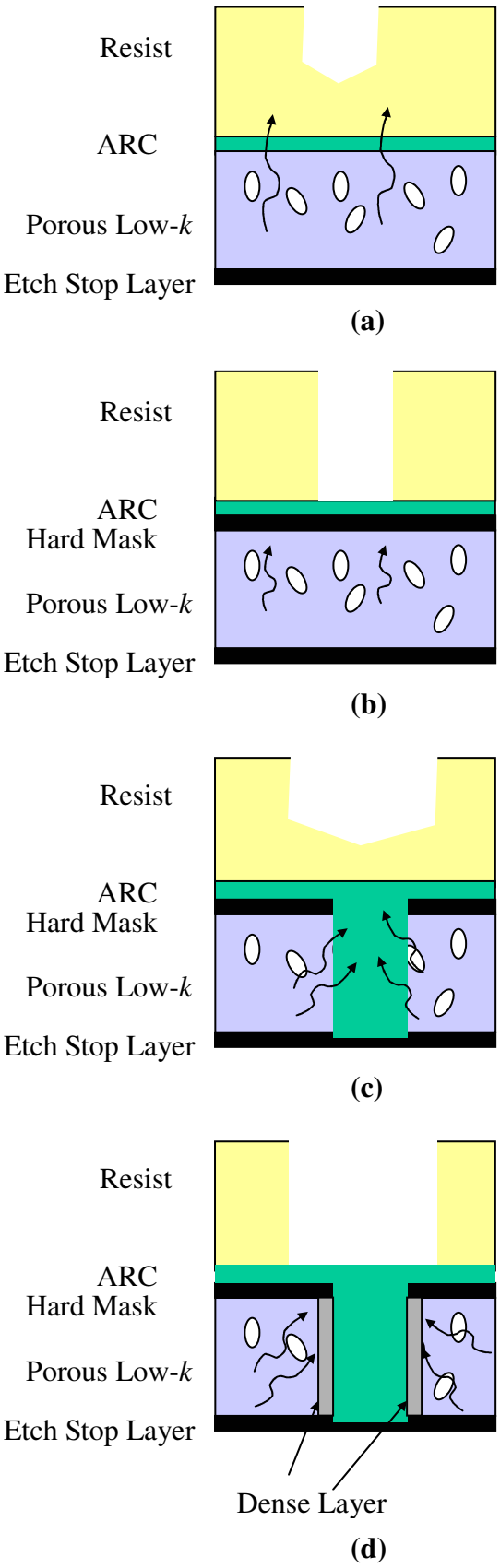

Fig. 4.12 (a) Photoresist poisoning in single damascene process. **(b)** Single damascene process with hard mask. **(c)** Photoresist poisoning in dual damascene process. **(d)** Dual damascene process with additional plasma treatment after via etch.

References

[1] K. H. Block and H. L. Rayle, Semicond. Intl. 6,115 (2002).

[2] P. T. Liu, T. C. Chang, H. Su, Y. S. Mor, Y. L. Yang, H. Chung, J. Hou, and S. M. Sze, J. Electrochem. Soc. 148, F30 (2001).

[3] J. N. Sun Y. F. Hu, W. E. Frieze, W. Chen and D. W. Gidley, J. Electrochemi. Soc. 150, F97 (2003).

[4] J. N. Sun, D. W. Gidley, T. L. Dull, W. E. Frieze, A. F. Yee, E. T. Ryan, S. Li, and J. Wetzel, J. Appl. Phys. 89, 5138 (2001).

[5] J. Bonitz, S. E. Schulz, T. Gessner, Microelectron. Eng. 70, 330 (2003).

[6] C. M. Whelan, Q. T. Le, F. Cecchet, A. Satta, J. J. Pireaux, P. Rudolf, and K. Maex, Electrochem. Solid-State Lett. 7, F8 (2004).

[7] P. D. Rouffignac, Z. W. Li, and R. G.. Gordon, Electrochem. Solid-State Lett. 7, G306 (2004).

[8] S. Y. Lee, Y. B. Kim, and J. S. Byun, J. Electrochem. Soc. 150, G58 (2003).

Chapter 5. Conclusion

In our study, the correlation between porosity and mechanical properties of porous low-*k* thin films and the effects of NH_3 plasma treatment on enhancement of mechanical properties of porous low-*k* thin films have been investigated.

The results in Chap. 3 show that higher porosity leads to lower Young's modulus and hardness. The value of Young's modulus and hardness will drop abruptly when the porosity exceeds 25%, a point where nano-pore structure changes from closed cells to interconnected pores. The result is consistent with the result obtained from curve fitting by semi-empirical equations.

It has been shown in this work that NH_3 plasma treatment can enhance the mechanical properties of MSQ-based porous low-*k* thin films (e.g., ZIRKON LK2200^{TM} porous low-*k* thin films). The plasma treatment results in carbon-depletion and nitrogen-incorporation region (less than 200 nm) in the porous low-*k* thin films. After the plasma treatment, the mechanical properties of porous low-*k* thin films were enhanced because the plasma treatment formed a thin non-porous dense layer (~10 nm thickness range) on top of the carbon-depleted region (as revealed by nano-indentation and PALS characterizations) by changing the near surface structure without affecting the whole porous structure of the thin film. The dense surface layer has higher Young's modulus and hardness than the porous low-*k* thin film. With the formation of the dense surface layer, the increased young's modulus and hardness would make the porous low-*k* thin films more compatible with CMP and packaging processes. Furthermore, the dense

surface layer sealed the porous surface. The sealing of the porous surface should be helpful in improving the integrity of a thin Cu diffusion barrier (e.g., Ta) formed on the porous low-*k* films and preventing photoresist poisoning during dual-damascene process for low-*k*/Cu integration.

The comparative study on JSR LKD5109^{TM} porous low-*k* thin films (also MSQ-based) further showed that NH_3 plasma treatment had the same beneficiary effect, i.e., improving the mechanical properties of the porous low-*k* films even though the nano-pores in the films are completely interconnected. However, it was found that the surface of NH_3 plasma-treated LKD5109 ^{TM} porous low-*k* thin film was not sealed completely, probably due to the high interconnectivity of the nano-pores in the films.

To summarize, we have shown that (1) the mechanical properties of the porous low-*k* films drastically deteriorates when the porosity of the films exceeds a certain critical value, a point where nano-pore structure changes from closed cells to interconnected pores; (2) NH_3 plasma treatment improves the mechanical properties of MSQ-based porous low-*k* thin films effectively by forming a thin hard dense layer (non-porous) on the surface of the films, but without changing chemical, structural, and physical properties in the bulk region of the films.